Title

Non-pharmacological Strategies to Suppress Triggers of Cardiac Arrhythmias by Targeting L-Type Ca2+ Channels

Author

Suriany, Silvie

Publication Date

2014

Peer reviewed|Thesis/dissertation

UNIVERSITY OF CALIFORNIA

Los Angeles

Non-pharmacological Strategies to Suppress Triggers of Cardiac Arrhythmias by Targeting L-Type Ca^{2+} Channels

A thesis submitted in partial satisfaction

of the requirements for the degree

Master of Science in Integrative Biology and Physiology

by

Silvie Suriany

2014

ABSTRACT OF THE THESIS

Non-pharmacological Strategies to Suppress Triggers of Cardiac Arrhythmias

by Targeting L-Type Ca^{2+} Channels

by

Silvie Suriany

Master of Science in Integrative Biology and Physiology

University of California, Los Angeles, 2014

Professor Riccardo Olcese, Co-Chair

Professor David L. Glanzman, Co-Chair

Sudden cardiac death is one of the major leading causes of death in the United States, affecting about 300,000 people annually on average. Cardiac arrhythmias and ventricular fibrillation can be triggered, at the cellular level, by the presence of aberrations of the cardiac action potential (AP) known as early afterdepolarizations (EADs). EADs are single or multiple voltage oscillations largely induced by the reactivation of L-type Ca^{2+} currents ($I_{Ca,L}$) during phase 2 and phase 3 of a cardiac AP. Our recent studies using dynamic clamp techniques have suggested that EADs and their arrhythmogenic consequences can be potently suppressed by subtle reduction the $I_{Ca,L}$ current non-inactivating (pedestal) component and/or minimal changes (3-5 mV) in the voltage dependence of activation. Exploiting the modulatory effects of L-type Ca^{2+} channel (LTCC) auxiliary β_2 subunits on the non-inactivating component of $I_{Ca,L}$, we sought to

investigate the effects of knocking down $Ca_v\beta_2$ subunit expression levels in rabbit ventricular myocytes in the presence of an oxidative stress known to trigger EADs (H_2O_2). We hypothesized that reducing the expression level of endogenous $Ca_v\beta_2$ decreases the probability of EAD occurrence in cardiomyocytes exposed to H_2O_2. Using an adenoviral infection to deliver a short hairpin RNA (shRNA) specific for targeting $Ca_v\beta_2$ that inhibits its gene expression by binding to its mRNA transcripts, our results showed that myocytes expressing less $Ca_v\beta_2$ mRNA exhibited no EADs; whereas, the control myocytes infected with GFP alone as a control group were more susceptible to EAD occurrence in 0.6 mM H_2O_2. These results suggest that $Ca_v\beta_2$ could be a potential target for gene therapy and could give insights to other therapeutic strategies that could possibly be implemented.

The thesis of Silvie Suriany is approved by

Alan D. Grinnell

David L. Glanzman, Committee Co-Chair

Riccardo Olcese, Committee Co-Chair

University of California, Los Angeles

2014

TABLE OF CONTENTS

Page

I. **Symbols & Abbreviations**……vi

II. **Acknowledgements**……vii-viii

III. **Introduction**
1. Cardiac function.....…….1
2. The cardiac action potential..……..2
3. Early afterdepolarizations and their relevance to cardiac arrhythmias……4
4. L-type Ca^{2+} channel (LTCC): structure, function and subunit composition……...…5
5. Role of β subunits in modulation of LTCC biophysical properties…….7
6. Dynamic clamp used to study the biophysical properties of LTCC.....…8
7. RNA interference for gene-silencing……10
8. Computational and genetic strategies for suppressing EADs……....11

IV. **Materials and Methods**
Myocyte isolation……..…….……12
Adenoviral construct…….…….……13
Myocyte culture and infection…….……..13
Electrophysiology……..14
Real-time polymerase chain reaction…….……16
Dynamic clamp……..16
Data analysis……..17

V. **Results**
Reducing the non-inactivating component (pedestal current) of $I_{Ca,L}$ abolished EADs…18
Various $Ca_v\beta$ subunit isoforms affect $I_{Ca,L}$ biophysical properties differently…...…...…19
Rabbit ventricular myocytes infected with an adenovirus containing $Ca_v\beta_2$ shRNA showed reduced levels of $Ca_v\beta_2$ mRNA transcripts.....……..……20
Down-regulation of $Ca_v\beta_2$ subunits in rabbit ventricular myocytes prevents EAD formation……21

VI. **Discussion**…….24

VII. **Limitations**……27

VIII. **Figures**……...28

IX. **Bibliography**……40

Symbols & Abbreviations

AP: action potential

APD: action potential duration

AV: atrioventricular

$Ca_V\beta$: β subunit of LTCC

DADs: delayed afterdepolarizations

EADs: early afterdepolarizations

LTCC: L-type Ca^{2+} channel

$I_{Ca,L}$: L-type Ca^{2+} current

RTXI: real-time experimental interface

SA: sinoatrial

SCD: sudden cardiac death

SERCA: sarco(endo)plasmic reticulum Ca^{2+}-ATPase

shRNA: short hairpin RNA

SR: sarcoplasmic reticulum

VF: ventricular fibrillation

Vm: membrane potential

ACKNOWLEDGEMENTS

I would like to thank Marina Angelini, Nicoletta Savalli, Antonios Pantazis, and Taleh Yusifov from the Olcese laboratory for their generous help and support these past couple of years. I would like to express my appreciation to my committee chair, Riccardo Olcese, for giving me the privilege of being a part of his lab and for mentoring me through the years. He has pushed me to put in the best I could in what I do; and with that encouragement, I managed to accomplish my project. Along with him are David Glanzman and Alan Grinnell who willingly supported me in getting my project successfully completed. Without the three of them, I would not have been able to achieve all that I have thus far. Roshni Madhvani has also played a huge part in my project by guiding me through the training I needed to carry out the project. I am very thankful that she kindly agreed to let me work with her on this arrhythmia project and continued the project even after she graduated. I would also like to thank our collaborator James N. Weiss and members of his laboratory, Rahil Patel and Pauline Morand, for helping me with the myocytes isolations.

Finally, I would like to acknowledge with deepest gratitude the support of my family, friends in Grace on Campus at UCLA, friends at Grace Community Church, and friends at International Evangelical Church in Los Angeles. Their encouragement for me has been a great fuel as I strived to finish my graduate program. They have consistently been there for me, reminding me to be a faithful steward of the tasks that I have been given in school and outside, to make me the person that I am today. I am very grateful for the small and big parts that each of the people mentioned here has played in my life.

Part of the work presented in this thesis has been submitted for publication and is currently under review on The Journal of General Physiology, titled "Importance of the Late Component of the L-type Ca^{2+} current in the Etiology of Cardiac Early Afterdepolarizations."

Roshni V. Madhvani[1], Marina Angelini[1], Yuanfang Xie[7], Antonios Pantazis[1], Silvie Suriany[1], Nils P. Borgstrom[5], Alan Garfinkel, [2,3,4,5], Zhilin Qu[2,5], James N. Weiss[2,3,5] and Riccardo Olcese[1,3,5,6]

[1]Division of Molecular Medicine - Department of Anesthesiology, Departments of [2]Medicine (Cardiology), [3]Physiology, [4]Integrative Biology and Physiology, [5]the Cardiovascular Research Laboratory, [6]the Brain Research Institute, David Geffen School of Medicine at University of California, Los Angeles, CA 90095-7115, USA, [7]Department of Pharmacology, UC Davis, CA, USA.

Introduction

Sudden cardiac death (SCD) is one of the major leading causes of death in the United States, accounting for about 300,000 to 400,000 deaths annually. SCD is often caused by cardiac arrhythmias that lead to the heart being unable to pump blood efficiently to the body. Among the many types of arrhythmias are ventricular fibrillation (VF), ventricular tachyarrhythmia, and torsade de pointes (TdP). Cardiac arrhythmias could lead to SCD as rapidly as within minutes. For decades, many studies have sought to understand the mechanisms of these arrhythmias in attempt to develop therapeutic strategies to suppress them. One commonly studied mechanism underlying VF is an abnormal electrical oscillation of the cardiac action potential (AP) referred to as an early afterdepolarization (EAD) (Cranefield *et al*., 1972; Sato *et al*., 2009; Weiss *et al*., 2010). EADs occurring at the cellular level could propagate through the heart and generate an abnormal wave of depolarization that disrupts the previously synchronized heartbeat, leading to VF. To better characterize EADs, many groups have been studying more closely the biophysical properties of various voltage gated protein channels governing the generation of normal cardiac AP. By understanding the mechanisms of EAD genesis, potential clinical therapeutic strategies are being developed and explored.

1. Cardiac function

The heart is a four-chambered unit that works to pump blood to the body. The ability of the heart to pump blood efficiently is dependent on the rhythmic electrical activity of the cardiomyocytes. The electrical activity in the heart is initiated spontaneously by the pacemaker cells residing in the sinoatrial (SA) node (Maltsev *et al.,* 2006). This electrical activity is recorded as a depolarization wave that propagates from the SA node to the atrioventricular (AV) node, then

down the bundles of His and the Purkinje fibers (Fig. 1A). A tight regulation of this electrical conducting system is critical for the synchronous contraction of both the atria and ventricles in order for blood to be pumped efficiently to the lungs for oxygenation and to the body for delivery of oxygen and nutrients. The electrical excitation of the heart allows Ca^{2+} ions to flow into the individual cardiomyocytes, which subsequently induce sarcoplasmic reticulum (SR) Ca^{2+} release to increase overall intracellular Ca^{2+} (Fig. 1B). The cytoplasmic Ca^{2+} allows for the binding of actin and myosin filaments in the cell, initiating muscle contraction that functions in the whole heart to empty the blood from the ventricles to the rest of the body. After the blood has been ejected from the ventricles, the ventricles need to relax for the next filling and ejection of blood to occur. The relaxation of the heart depends on the removal of the intracellular Ca^{2+} to reset the concentration to baseline, which could be achieved in two ways: Ca^{2+} being recycled back into the SR or Ca^{2+} being pumped out of the cell into the extracellular space. The excitation and contraction of the cardiac tissue have to cease before the processes could repeat for the next cycle of blood pumping could begin again.

2. The cardiac action potential

An action potential (AP) refers to the change in the electrical potential across a membrane of a an excitable cell. The shape of the AP is dependent on the overall interactions between the various inward and outward ionic conductances over the course of the AP (Fig. 2) (Ravens & Cerbai, 2008). The action potential shapes are different in various parts of the heart. The pacemaker cells in the SA node and AV node have pacemaker potentials that are self-generative and spontaneous with a slow depolarization toward the threshold potential. These pacemaker potentials are important because they are the main determinant of the heart rate. The upstroke of the pacemaker potential is mainly due to Ca^{2+} influx and the repolarization of the AP is due to

outward K^+ currents (Shibata & Giles, 1985). In ventricular myocytes, the action potential is governed by ionic currents different from those of the pacemaker potential. It begins when excitation from adjacent cardiomyocytes activates voltage-gated Na^+ channels (VGSCs), which leads to an increase in the membrane permeability to Na^+ ions, causing the flow of inward I_{Na+}. This initial influx of Na^+ causes a depolarization of the membrane potential (Vm). The depolarization induces a positive feedback that activates even more VGSCs, contributing to a rapid acceleration of Na^+ conductance. This fast depolarization gives rise to phase 0, the rapid upstroke of the AP (Fig. 2). Following the membrane depolarization, VGSCs begin inactivating, causing a reduction in inward I_{Na}. At this time, fast-activating-inactivating voltage-gated K^+ channels generate a transient outward K^+ currents (I_{to}) that produce the transient rapid repolarization potential observed during phase 1. A plateau phase (phase 2) follows as inward L-type calcium currents ($I_{Ca,L}$) activate, balancing the combination of several outward K^+ currents (Fig. 2). The plateau phase during which Ca^{2+} enters the cell accounts for the ~300 ms-long AP duration (APD) of the heart, which is longer than neuronal and skeletal muscle APs. This APD is essential for the prevention of electrical re-excitation and tetanic contraction in the heart, which could inhibit relaxation needed for the filling of blood prior to ejection (Bers, 2001). The influx of Ca^{2+} through L-type Ca^{2+} channels (LTCC) during this plateau phase has several implications in the cell. The Ca^{2+} that enters the cell induces a phenomenon known as Ca^{2+}-induced Ca^{2+} release by activating ryanodine receptors (RyRs) on the SR, which allows Ca^{2+} to be released into the cytoplasm (Bers, 2002; Bers & Guo, 2005). The overall increase in intracellular [Ca^{2+}] activates cardiomyocyte contraction. Furthermore, Ca^{2+} also binds to Ca^{2+}-sensing protein, calmodulin, which interacts with LTCC, mediating Ca^{2+}-dependent LTCC inactivation (Peterson *et al*., 1999). LTCC is also inactivated in a voltage-dependent manner. As $I_{Ca,L}$ inactivates, I_K

takes over and drives the repolarization of the Vm in phase 3. Intracellular Ca^{2+} is pumped back out to the extracellular space by Na^{+}/Ca^{2+}-exchanger (NCX) and restored back in the SR by sarco(endo)plasmic reticulum Ca^{2+}-ATPase (SERCA) at the end of each muscle contraction (Ottolia *et al*., 2013). The Vm of the cell finally repolarizes its resting potential before the next action potential could take place again for the next heartbeat.

3. Early afterdepolarizations and their relevance to cardiac arrhythmias

The electrical activity in the heart can be arrhythmic when there is an abnormality in the structure and function of the myocardium. Major causes of cardiac arrhythmias are ventricular fibrillation (VF) and ventricular tachycardia (VT) (John *et al*., 2012). One mechanism underlying VF and VT is a premature excitation induced in a ventricular cardiomyocyte that generates an extra wave of depolarization, which could collide with the oncoming wave conducted from the SA node, so producing a wave break. This collision subsequently generates spiral waves of electrical activity originating from the ventricles to the whole heart tissue, which prevents the heart from beating synchronously and ultimately reduces its ability to pump blood efficiently. At the cellular level, two commonly studied triggers of cardiac arrhythmias are delayed afterdepolarization (DAD) caused by premature Ca^{2+} release during diastole (Clusin, 2003), and early afterdepolarization (EAD) caused by a reverse of polarization during the repolarizing phase of the cardiomyocyte's Vm. In this study, I will be discussing the cellular mechanisms for EAD generation in rabbit ventricular myocytes.

EADs were first described by Cranefield and his colleagues in 1972 as they observed them in a bundle of Purkinje fibers of an intact cardiac tissue in canine (Cranefield *et al*., 1972). EADs were subsequently described as a form of "triggered activity" in myocardium caused by the

transition from a normal to a rapid, asynchronous electrical activity of the heart (Cranefield & Aronson, 1974; Cranefield, 1977). At the cellular level, this triggered activity often refers to the secondary depolarization that occurs during the repolarization phase (late phase 2 and phase 3) of a cardiac AP (Weiss *et al*., 2010). Formation of EAD is largely dependent upon the net ionic conductance governing those phases. An increase in the inward $I_{Ca,L}$ and/or a reduction in the outward I_K could alter the repolarization phase such that the net increase in inward current eventually reverses the repolarization of the membrane potential (Weiss *et al*., 2010). This abnormal imbalance of the net ionic currents also often results in the lengthening of AP duration (APD) (January *et al.*, 1988). The increase in $I_{Ca,L}$, which could be attributed to the reactivation of $I_{Ca,L}$, has been shown in previous work as a key player in EAD genesis (January & Riddle, 1989). $I_{Ca,L}$, when reactivated in cardiomyocytes, can induce a regenerative inward current that depolarizes the cell membrane potential, forming the upstroke of EADs (Weiss *et al*., 2010). The reactivations of $I_{Ca,L}$ normally occur approximately between -40 to 0 mV, as shown in fig. 3. This voltage range is also often referred to as the "window current" region of $I_{Ca,L}$ (January & Riddle, 1989). It is the region of overlap between the steady state activation and inactivation curves of $I_{Ca,L}$, the shaded area in fig. 3A. Steady state curves of $I_{Ca,L}$ show the voltage dependency of LTCC activation and inactivation over a range of membrane potentials. As cardiac AP repolarizes into this range of potential, a fraction of the LTCC can recover from inactivation and be reactivated, thereby conducting inward Ca^{2+} that induces a secondary depolarization that can propagate, resulting in a premature beat in the myocardium (Hirano *et al*., 1992).

4. L-type Ca^{2+} channel (LTCC): structure, function and subunit composition

Many different types of voltage-gated calcium channels (VGCCs) are found in different cell types, all functioning to mediate Ca^{2+} influx upon membrane depolarization in response to an

action potential. They play critical roles in the normal physiological functions of the cells such as enzymatic activities, muscle contractions, hormone secretion, neurotransmitter release during a synaptic transmission, and gene expression (Yang & Berggren, 2006; Flavell & Greenberg, 2008; Catterall & Few, 2008; Caterall, 2011). In cardiac ventricular myocytes, L-type Ca^{2+} channels (LTCCs) are more ubiquitous than T-type calcium channels (TTCCs) (Ono & Iijima, 2009). TTCCs are more commonly found in the pacemaker cells residing in the conduction system. Unlike TTCCs that conduct transient inward Ca^{2+} currents, LTCCs activate at a more depolarized voltage and have slower voltage-dependent inactivation that contributes to their long lasting conducting property (Tsien *et al*., 1988; Ono & Iijima, 2009). LTCCs are crucial in maintaining the time course of a cardiac AP, in providing the passageway of Ca^{2+} entry into the cell, and ultimately in excitation-contraction coupling of a cardiac myocyte (Bers, 2002). Ca^{2+} entering the cell during an AP triggers SR release of Ca^{2+} via Ca^{2+}-induced Ca^{2+}-release phenomenon.

LTCCs were first known as dihydropyridines receptors attributing to their sensitivity to dihydropyridines. The heteromultimeric LTCCs were first cloned from rabbit skeletal muscle by Tanabe and colleagues in 1987 (Tanabe *et al*., 1987). LTCCs are composed of an ion-conducting pore α_1 subunit and auxiliary subunits $\alpha_2\delta$, β, and γ as shown in fig. 4A. The pore-forming α_1 subunit contains four non-identical repeats, each consisting of six membrane-spanning segments (S1-S6). The four S4 segments are referred to as the main voltage-sensing region of the channel, containing positively charged amino acids, which are displaced in response to a change in Vm. The P-loops, located between S5 and S6 segments, form the actual pore of the channel that is selective for Ca^{2+}. Near the carboxy-terminal domain is the IQ motif where calmodulin, a Ca^{2+}

sensor, binds. This Ca^{2+}/calmodulin sensor drives LTCC Ca^{2+}-dependent inactivation, which is important for regulating the level of Ca^{2+} during cardiac AP (Caterall, 2011).

The α_1 subunits also normally interact with at least the $\alpha_2\delta$ and β subunits that regulate LTCC functions (Hosey *et al*., 1996). Singer and colleagues showed that expression of α_1 subunit alone contributes to functional LTCCs (Singer *et al.*, 1991), while coexpression with $\alpha_2\delta$ and β subunits increases the current conductance by promoting trafficking of α_1 subunit to the plasma membrane (Dolphin, 2012). As illustrated in fig. 4B. Most of $\alpha_2\delta$ subunit is extracellular, with the δ part anchored to the plasma membrane via glycophosphatidylinositol (Davies *et al*., 2010; Caterall, 2011). δ and α_2 are connected via a disulfide bridge as shown in fig. 4B. Much less is known about γ subunits; their structure and functions are still open for investigation. On the other hand, the intracellular β subunits of LTCC ($Ca_v\beta$) have been extensively studied. They are localized near the plasma membrane and have been demonstrated as traffic regulators of the pore-forming α subunit to the plasma membrane (Dolphin, 2003, 2012; Buraei, 2013). Additionally, to modulate the biophysical properties of LTCC, $Ca_v\beta$ have been shown to modulate Ca^{2+} channel biophysical properties by associating with the cytoplasmic linker between repeat I-II of the α_1 subunit known as α-interaction domain (AID) (Arikkath & Campbell, 2003). The profound modulation of the biophysical properties could affect the overall size of the "window current" region that has been implicated in EAD formation.

5. Role of β subunits in modulation of LTCC biophysical properties

Aside from its role in LTCC trafficking, $Ca_v\beta$ have been shown to play a role in modulation of biophysical properties of LTCC (Birnbaumer *et al*., 1998; Dolphin, 2003, 2012). Specifically, $Ca_v\beta$ increase overall $I_{Ca,L}$, enhance the activation kinetics, and shift the voltage-conductance

relationship toward more hyperpolarized potentials in *Xenopus* oocytes (Perez-Reyes *et al*., 1992). A study done in rat ventricular myocytes has demonstrated that four isoforms of $Ca_v\beta$ subunits, namely β_1, β_2, β_3, and β_4, contribute to an increase in the open probability of LTCC to different degrees (Colecraft *et al*., 2002). Each β subunit is encoded by different genes with each having its own alternative splicing (Buraei & Yang, 2013). The various isoforms, when coexpressed with human α_{1E}, have been shown to modulate inactivation of VGCCs expressed in *Xenopus* oocytes (Olcese *et al*., 1994) Among the different $Ca_v\beta$ subunits, $Ca_v\beta_{2a}$ subunit seemed to produce the greatest enhancement in the current density compared to all other β isoforms (Colecraft *et al*., 2002). $Ca_v\beta_{2a}$ subunit increases the inactivation time in LTCCs (Caterall, 2000) and shifts the half-activation potential of LTCC to more negative potentials (Neely *et al*., 1993). Additionally, increased expression of β_{2a} has been seen in failing human hearts, which are prone to arrhythmias, and it has also been shown to play a role in pathological membrane excitability leading to cell death in adult cardiomyocytes (Hullin *et al*., 2007). Among the various β subunits, β_{2a} subunit has been shown to have the most profound enhancement on the open probability of L-type Ca^{2+} channels (Buraei & Yang, 2013). Additionally, Gudzenko and his colleagues have also shown that channels with β_{2a} had higher non-inactivating pedestal component of the current as compared to channels with β_3 (Gudzenko *et al*., 2007).

6. Dynamic clamp used to study the biophysical properties of LTCC

The first recordings of currents from open ion channels in artificial bilayers were done in 1963 by Müller and Rudin (Müller & Rudin, 1963). The conventional technique that has been widely used to assess the electrical properties of cells, specifically ion channels, is the patch clamp. In 1980s, Neher and Sakmann used the concept of voltage clamp and invented a patch clamp that can be used to monitor and record single ion conductance (reviewed by Verkhratsky & Parpura,

2014). They received a nobel prize for pioneering this technique, which has been very valuable in physiological studies of ion channels even to this day. Several different ways of studying single ion channels include inside-out, outside-out, perforated, and whole-cell patches. The one used in our experimental recordings is a whole-cell patch, whereby an access to the intracellular space is obtained, recording multiple channels at once. Patch clamp is a desirable tool to record channel activities as it has a low background noise crediting to the very tight seal (>1GΩ) between the micropipette and the cell membrane known as a gigaseal. A powerful evolution of the patch clamp is the dynamic clamp technique that combines electrophysiological recordings and mathematical modeling in real-time. This allows for the introduction of a virtual (computer-simulated) ionic current into a cell to test its impact on the cell electrical properties and excitability. The concept of dynamic clamp was first demonstrated in a study of artificial electrical coupling between isolated rabbit ventricular myocytes in a whole-cell clamp (Tan & Joyner, 1990). They did a simulation of two cells with a variable coupling resistance without physically coupling them to observe changes in the properties of each cell individually as a result of artificially providing electrical coupling between them (Tan & Joyner, 1990). Dynamic clamp has since been used by several groups in their studies, giving insights to the behavior of different excitable cells (Wilders, 2006; Berecki *et al*., 2005, 2006, 2007; Madhvani *et al.*, 2011). We took advantage of this hybrid experimental-computation system to explore with great precision the different biophysical properties of $I_{Ca,L}$ that could potentially serve as a therapeutic target for EAD suppression. In our experiments, a virtual $I_{Ca,L}$ with programmable properties is injected into a cell in real time to study its effects on action potential (AP) characteristics without altering other existing ionic conductance in the cell (Fig. 5). Using this technique, our laboratory was able to previously show that a 4-5 mV leftward shift in half-inactivation potential and a 4-5 mV

rightward shift in half-activation potential, both of which lower the area encompassing the window current region, potently abolished EADs in rabbit ventricular myocytes (Madhvani *et al.*, 2011). Their studies also supported the relevance of $I_{Ca,L}$ in EAD formation and showed that by manipulating only the $I_{Ca,L}$ biophysical properties, EADs could be abolished, even though there may be many other ionic currents involved in the initial EAD genesis (Madhvani *et al.*, 2011). These findings suggest that LTCC could be a potential target for therapy to suppress EADs and eventually arrhythmias.

7. RNA interference for gene-silencing

The idea of using a complementary sequence of a messenger RNA to inhibit translation was first demonstrated in Escherichia coli in the early 1980s (Mizuno *et al*., 1984). This concept has been adopted by many studies as a tool for understanding gene function. RNA interference is subsequently discovered and defined as a mechanism of specific gene-silencing at the post-transcriptional level mediated by small RNAs such as microRNA, small interfering RNA, and short hairpin RNA (shRNA) (Fire *et al*., 1998; reviewed in Deng *et al.*, 2014). This discovery by Fire and Mello was merited with a nobel prize in 2006. Among the few RNAi types, shRNA has been shown to be more effective and potent in silencing genes (reviewed in Deng *et al.*, 2014). Several studies have reported recombinant adenovirus as a great vector for mediating RNAi delivery for gene silencing (Benihoud *et al*., 1999; Hosono *et al*., 2004, 2005; Motegi *et al*., 2011). Adenoviruses are double-stranded non-enveloped replication-defective vectors that have been used for gene transfer in a variety of cell types (Kirshenbaum *et al*., 1993; Benihoud *et al*., 1999; Suckau *et al*., 2009; Li *et al*., 2012; Gupta *et al*., 2012). Taking advantage of this powerful tool, we designed an shRNA that targets $Ca_v\beta_2$ mRNA transcripts, with a recombinant adenovirus as a delivery system, to reduce their expression levels in rabbit ventricular myocytes.

We tested the hypothesis that a reduction in $Ca_v\beta_2$ subunit levels provides resistance against EAD formations under oxidative stress conditions (H_2O_2).

8. Computational and genetic strategies for suppressing EADs

In this thesis, I discuss the effects of the non-inactivating pedestal component of $I_{Ca,L}$ on EAD susceptibility in rabbit ventricular myocytes exposed to an oxidative stressor, H_2O_2, using dynamic clamp technique. Our results demonstrate that non-inactivating pedestal current plays a critical role in H_2O_2-induced EAD formation, and could be a potential target for genetic therapy. We subsequently tested the possible effects of knocking down $Ca_v\beta_2$ subunits in ventricular myocytes using an shRNA that targets specifically the $Ca_v\beta_2$ subunits. Our results showed that myocytes expressing lower levels of $Ca_v\beta_2$ subunits exhibited no EADs in the presence of H_2O_2. This suggests that knocking down $Ca_v\beta_2$ subunits could potentially increase resistance to EAD formation in cardiomyocytes, maintaining a normal AP duration as compared to the control myocytes. This could eventually lead to the prevention of arrhythmia-related cardiovascular diseases, by using a genetic therapeutic approach to manipulate the activity of the heart at a cellular level.

Materials and Methods

Ethical approval. All animal handling protocols were approved by the UCLA Institutional Animal Care and Use Committee and conformed to the Guide for the Care and Use of Laboratory Animals published by the US National Institutes of Health.

Myocyte isolation. Ventricular myocytes were isolated from three- or four-month-old male New Zealand white rabbits as previously described (Mahajan *et al.*, 2008a). The rabbits were first injected with heparin sulfate (1000 U) and sodium pentobarbital (100 mg/kg) intravenously. Adequacy of the anesthesia was confirmed by the lack of pedal withdrawal reflex, corneal reflex, and motor response to pain stimuli. Following excision, the heart was submerged in Tyrode's buffer solution containing (in mmol/L): 136 NaCl, 5.4 KCl, 1 $MgCl_2$, 0.33 NaH_2PO_4, 0.2 $CaCl_2$, 10 Glucose, and 10 HEPES adjusted to pH 7.4. Using a retrograde Langendorff perfusion system, the rabbit's excised heart was first perfused with Tyrode's solution until all blood was washed out thoroughly; then, Tyrode's solution containing 0.8mg/mL bovine serum albumin and 1.65mg/mL collagenase was constantly perfused for about 30 to 40 minutes to ensure sufficient digestion time. The enzyme-containing solution was washed out after the digestion time and the heart was submerged and mechanically torn apart with forceps in Tyrode's solution containing 0.2 mmol/L Ca^{2+}. The pieces of the tissue were swirled in the solution to aid cell dissociation. The dissociated myocytes were then washed several times in 1.8 mM Ca^{2+}-containing Tyrode's buffer solution using centrifugation to remove as much dead cells as possible following the isolation. The myocytes were either used directly for electrophysiological experiments or for culturing.

Adenoviral construct. We used recombinant adenoviruses as a gene expression system to deliver the gene coding for the shRNA targeting $Ca_v\beta_2$ mRNA transcripts. The shRNA sequence is 5'-AAAAAAACATGAGGCTACAGCATG AATTGGATCCAATTCAGCTGTAGCCTCATGTTTTTTT- 3'. This shRNA was subcloned into adenovirus plasmids under the human U6 promoter, which have been widely used to induce RNAi in mammalian cells. Within the same plasmid is a CMV promoter driving the expression of GFP. The adenovirus production was done following a protocol previously designed (Luo *et al*., 2007). As a control, another adenovirus plasmid containing just GFP without the shRNA construct was used. The viruses were first propagated in transfected HEK 293 cells and maintained at 5% CO_2, 37 °C in Minimum Essential Media (MEM) (Life Technologies) with Earle's salts and L-glutamine, supplemented with 5% fetal bovine serum (FBS), and 1% Penicillin-Streptomycin (pen/strep) antibiotic solution. The viruses were then purified from the HEK 293 cells once enough fluorescence of GFP was observed under fluorescence microscopy. The viral stocks were kept at -80°C to slow down their mortality rate.

Myocyte culture and infection. Autoclaved glass coverslips of 5 mm size (Warner Instruments) were coated with Geltrex (Invitrogen) and kept for about an hour in an incubator for cultures at 37°C with an atmosphere of 95% O_2 and 5% CO_2. Ventricular myocytes dissociated in 1.8 mM Ca^{2+}-containing Tyrode's buffer solution were subsequently washed in sodium bicarbonate buffered Medium 199 with Earl's salts, L-glutamine, 1% penicillin/streptomycin and 5% bovine serum (Cellgro) at pH of 7.3 to 7.4 that has been incubated at atmosphere of 5% CO_2 for at least an hour. Medium 199 contains all amino acids (except glutamine), vitamins, and containing (in mmol/L): 1.8 $CaCl_2$, 116 NaCl, 0.6 Na acetate, 1 $NaHPO_4$, 5.3 KCl, 0.8 $MgSO_4$. The myocytes were then plated at densities of about 10^4 cells/cm^2 for 3 to 4 hours prior to adenovirus infection

to allow them to attach to the coated coverslips. Right before the infection, the media in the dish containing attached myocytes was replaced with Medium 199 supplemented with 1X insulin-transferrin-selenium (ITS) and 15 μM Blebbistatin, for nutrients and reduced contraction. One dish that served as a control was prepared for GFP-only virus infection, while another dish was prepared for β_2 shRNA-GFP virus infection. ~10 μL of the virus stock is added to 1 mL of medium in a dish.

Electrophysiology. For dynamic clamp experiments, freshly dissociated ventricular myocytes bathed in Tyrode's buffer solution were then patched under whole-cell current clamp. The myocytes were first patched in Tyrode's solution before 0.6 mM H_2O_2 was perfused to induce EADs. Once EADs were seen in consecutive APs, Tyrode's solution containing 20 μL nifedipine and 0.6 mM H_2O_2 was perfused. The 20 uL nifedipine was used to block $I_{Ca,L}$. Once the nifedipine effect showed, the dynamic clamp was turned ON. The charges (q) on the membrane was measured by taking the integral of the capacitative current by using the program Analysis, the capacitance was calculated using the equation C = q/V, which is then inputted into the parameters shaping the virtual $I_{Ca,L}$ on real time experimental interface (RTXI) for each cell. V is the voltage at which we recorded the capacitative current, V= 5 mV. Cells were paced at 6 s pacing cycle length.

Cultured myocytes: Whole-cell current clamp was conducted between 36-48 hr after the myocytes were infected with the viruses. All recordings were measured using AxoPatch 200B (Axon Instruments). Whole-cell patch-clamp recordings were performed using electrodes with tip resistance of 1-3 MΩ borosilicate pipettes. The pipette solution contained (in mmol/L): 110 K-Aspartate, 30 KCl, 5 NaCl, 10 Hepes, 0.1 EGTA, 5 MgATP, 5 creatine phosphate, 0.5 cAMP, adjusted to pH 7.2. All electrophysiological experiments were performed at 34-36°C. 0.6

mmol/L of H_2O_2 was used as an oxidative stress to induce EAD in the myocytes. $I_{Ca,L}$ recordings were done using the Tyrode's buffer and pipette solutions described above, with the following changes: 10 μmol/L tetradotoxin (TTX) was added to the extracellular solution to eliminate Na^+ conductance, and K^+ was replaced with Cs^+ to block K^+ conductance. $I_{Ca,L}$ was calculated by subtracting the current recorded after addition of 20 μmol/L nifedipine from the total current. The steady state activation and inactivation curves were constructed as previously described (Madhvani *et al*., 2011). The steady state activation curves: divide the peak *I–V* curve by the driving force to calculate conductance (*G*) and divide *G* by G_{max}. The steady state inactivation curves were constructed by graphing the normalized peak current during a test pulse at 10 mV after a 300 ms inactivating pulse at different voltages. Boltzmann distribution fitting was used to estimate the half-activation/inactivation potential of the steady state activation/inactivation curves. The Boltzmann distribution fitting for steady state activation is given by the following equation: $(I_{max})/(1+EXP((V_{half}-Vm)/slope))$; while the steady state inactivation is given by the following equation: $(I_{max}-I_{min})/(1+EXP((Vm-V_{half})/slope))+I_{min}$.

Oocytes: *Xenopus* oocytes of stages V-VI were prepared and injected with 0.05 µl of cRNA containing 0.1 to 1 mg/mL of $\alpha_{1c}/\alpha_2\delta$, $\alpha_{1c}/\alpha_2\delta/\beta_3$, and $\alpha_{1c}/\alpha_2\delta/\beta_{2a}$ in equal molarity. The oocytes were then incubated for 4-7 days prior to electrophysiological experiments at 18°C in an amphibian saline solution containing 50 µg/mL gentamycin (Invitrogen). Immediately preceding each experiment, each oocyte was injected with 0.1 µl of 50 mmol/L BAPTA, which is 1,2-Bis(2-aminophenoxy)ethane-N,N,N′,N′-tetraacetic acid tetrakis (acetoxymethyl ester) (Sigma). Cut-open oocyte voltage clamp technique was used to obtain electrophysiological recording of the injected oocytes. The oocytes were bathed in a solution containing (in mmol/L): 105 NaMES, 10 HEPES, 10 CaMES, and 0.1 Ouabain, adjusted to pH 7.0. The internal solution contained 110

mmol/L K-Glutamate and 10 mmol/L HEPES, also adjusted to pH 7.0. Steady state activation curves were fit to a Boltzmann given by the following: $(I_{max}) / (1+EXP(z(Vm-V_{half})/(RT/F)))$. Steady-state inactivation curves were fit with a Bolztmann distribution given by the following equation: $(I_{max}-I_{min})/(1+EXP(z(Vm-V_{half})/(RT/F))) + I_{min}$.

Real-time polymerase chain reaction. We measured the mRNA transcript levels of β_{2a}, β_{2b}, β_3 and GAPDH. Both β_{2a} and β_{2b} were measured because the shRNA is not specific for either. β_3 was measured to monitor any potential compensation in the cell. RNA was isolated from myocytes infected with GFP only and myocytes infected with β_2 shRNA-GFP following 24-48 hr of culturing. The isolation was done using Trizol (Invitrogen) and the RNAs were subsequently reverse-transcribed with gene specific primers using the Omniscript RT kit (Qiagen). The primer sequences used were as follows: β_{2a} forward primer (5'-GTA CGC GCG AGT CCT GGG C-3'), reverse primer (5'-GTC GCT CAG CTT CTC TGC GC-3'); β_{2b} forward primer (5'-GCA GCT CGC TCG TGC CTG C-3'), reverse primer (5'-CAG GAG CGA CGA GAG CTG AG-3'); β_3 forward primer (5'-AGA CTA TGC GGA CGC CTA CCA-3'), reverse primer (5'-GCT AGG GTG GGA ACA TCA GGA-3'); GADPH forward primer (5'-CCT GCA CCA CCA ACT GCT TAG-3'), reverse primer (5'-ATG ACC TTG CCC ACG GCC TT-3'). GAPDH transcript levels were used as a baseline for normalization of the relative fluorescence obtained from RT-PCR.

Dynamic clamp. This technique combines mathematical model and biological systems for electrophysiological allows for a computer-simulated ionic conductance to be injected into a live cell in real-time using a real-time experimental interface (RTXI). The mathematical model of the cardiac AP we used for our experiments computes all Ca^{2+}-dependent ionic conductances including $I_{Ca,L}$, the fast sodium current I_{Na}, the Na^+/K^+ pump current I_{NaK}, the Na^+/Ca^{2+} exchange current I_{NCX} and the Ca^{2+}-dependent slow component of the delayed rectifier potassium channel

$I_{Ks,}$ as described previously (Mahajan *et al.*, 2008; Madhvani *et al.*, 2011). Briefly, the Ca^{2+} flux into the cell due to $I_{Ca,L}$ is given by

$$J_{ca} = g_{ca} P_o i_{ca} \quad ; \qquad i_{ca} = \frac{4 P_{ca} V_m F^2}{RT} \frac{Cse^{2a} - 0.341[Ca^{2+}]_o}{e^{2a} - 1}$$

where *Cs* is the submembrane concentration in units of mmol/L. P_{Ca} is the permeability of Ca (0.0054 m/s), V is the voltage, F is the Faraday's constant, T is temperature. P_o was formulated as

$$P_o = d \cdot f \cdot q$$

where *d* is the voltage-dependent activation gate, *f* is the voltage-dependent inactivation gate and *q* is the Ca^{2+}-dependent inactivation gate.

Data Analysis. All data acquired on G-Patch were analyzed on Analysis, both of which are custom-made.APD at 90% repolarization (APD_{90}) was measured by using a custom-made software, AP analyzer. EAD amplitude was calculated by taking the difference in Vm from the inflection point where dV/dt is 0 to the peak of the EAD where dV/dt is also 0. Only the EAD having the largest voltage excursion was included in the analysis for cells displaying APs with multiple EADs. % EAD is reported as the percentage of APs that displayed at least one EAD. Error bars show the standard error of the mean (SEM). The control parameters in the $I_{Ca,L}$ formulation were determined by fitting formulated current to experimental nifedipine-sensitive $I_{Ca,L}$ records (Madhvani *et al.*, 2011) using Berkeley Madonna and then implemented for dynamic clamp in RTXI (*Lin et al.*, 2010) (www.rtxi.org). The sampling/computation frequency was 10 kHz.

Results

Reducing the non-inactivating component (pedestal current) of $I_{Ca,L}$ abolished EADs.

As discussed in the introduction, the voltage range within which a fraction of LTCC reactivates, the "window current" region has been shown to play a major role in EAD genesis (January & Riddle, 1989). The "window current" region is determined by the various biophysical properties of LTCC, one of them being the non-inactivating component. Madhvani and colleagues have previously shown that H_2O_2 increases the non-inactivating component of L-type Ca^{2+} currents ($I_{Ca,L}$) from 3% to 9-10% (Madhvani *et al*., 2011). To determine the relevance of the non-inactivating pedestal $I_{Ca,L}$ on EAD genesis, we used dynamic clamp to alter the pedestal current while keeping all other properties unchanged. Under current clamp condition, single rabbit ventricular myocytes were paced every 6s in Tyrode's buffer solution for about 5 min to record AP under control conditions. The solution in the recording chamber was replaced with Tyrode's buffer containing 0.6 mM H_2O_2. This maneuver induced a consistent EAD regime within ~10 minutes. H_2O_2 has been shown to induce the formation of EADs by lowering the repolarization reserve in myocytes through the enhancement of late I_{Na}, $I_{Ca,L}$, and the Na^+/Ca^{2+} exchanger (reviewed by Karagueuzian *et al*., 2013). After the induction of EADs, the endogenous $I_{Ca,L}$ was blocked with 20 μL nifedipine (with H_2O_2 still present) and replaced by a virtual $I_{Ca,L}$ generated under dynamic clamp by Ca channel model. To correctly scale the virtual $I_{Ca,L}$ to the size of the cell , cell capacitance was calculated and inputted into the model. Under dynamic clamp, a consistent EAD regime was reestablished and AP durations similar to those with endogenous $I_{Ca,L}$ were reconstructed. The results from dynamic clamp experiments show that reducing the $I_{Ca,L}$ "window current" region (i.e. the overlapping of the steady-state inactivation and activation curves, Fig. 3) by lowering the non-inactivating pedestal component of $I_{Ca,L}$ from 10% (the

baseline pedestal in the presence of H_2O_2, Madhvani *et al*., 2011) to 4% (Fig. 6A, B), results in a 100% elimination of EADs. Reducing the pedestal also restored normal AP morphology (Fig. 6C, D): the average action potential duration was reduced from 1.11±0.095s to 0.186±0.002 s (Fig. 6E, F) in myocytes still exposed to 0.6 mM H_2O_2.

In summary, based on these and our previous results, we conclude that the non-inactivating pedestal component of $I_{Ca,L}$, as well as its voltage dependency of activation and inactivation, can potentially be effective targets to suppress H_2O_2-induced EADs. Interestingly, modifications of $I_{Ca,L}$ biophysical properties that results in the reduction of the "window current" region seems to be a promising therapeutic intervention to suppress cardiac arrhythmias.

Various $Ca_V\beta$ subunit isoforms affect $I_{Ca,L}$ biophysical properties differently.

Olcese and colleagues have previously shown that different $Ca_v\beta$ modulatory subunits, when coupled with human α_{1E} Ca^{2+} channel as its pore-forming subunit, have different and profound modulatory effects on its activation and inactivation properties that alter the "window current" region (Olcese *et al*., 1994). We obtained similar results with LTCC when we coexpressed the α_{1c} and $\alpha_2\delta$ subunits of LTCC with either $Ca_v\beta_{2a}$ or $Ca_v\beta_3$ subunit or without any $Ca_v\beta$ in *Xenopus* oocytes and measured the steady state properties of each combination. The steady state curves in fig. 7 demonstrate that $\alpha_{1c}/\alpha_2\delta/\beta_{2a}$ subunits exhibit higher non-inactivating pedestal current than $\alpha_{1c}/\alpha_2\delta/\beta_3$ and $\alpha_{1c}/\alpha_2\delta$. The modulation on the electrophysiological properties of LTCC can be observed in the shift of the steady state activation curve to a more hyperpolarized potential with β subunits as compared to LTCC without any β subunits as shown in fig. 7. Our results suggest that the presence of β subunits itself increase the “window current” region by shifting the half-activation potential toward hyperpolarized potentials. Thus, $Ca_v\beta_{2a}$ likely

enhances the activation of $I_{Ca,L}$, as well as increase the probability of $I_{Ca,L}$ reactivation; in which both cases would lead to EAD formation. Interestingly, Ca^{2+} channel β_{2a} subunit expression has been shown to be elevated in cardiomyocytes in mice model of heart failure (Hullin *et al*., 2007), a condition known to favor EADs. Additionally, it has also been demonstrated that β_{2a} expression causes Ca^{2+} overload and induced arrhythmogenic EADs, which eventually led to cell death (Koval *et al.,* 2010). According to these findings, we hypothesized that lowering the overall levels of $Ca_v\beta$ subunits in ventricular myocytes may reduce the size of "window current" region and potentially be effective to suppress EADs.

Rabbit ventricular myocytes infected with an adenovirus containing $Ca_v\beta_2$ shRNA showed reduced levels of $Ca_v\beta_2$ mRNA transcripts.

As β_2 subunit displays properties that appears to favor $I_{Ca,L}$ reactivation that leads to EAD genesis, we tested the hypothesis that a reduction in β_2 subunit expression level in rabbit ventricular myocytes lowers the probability of H_2O_2-induced EAD occurrence. Overall, we expected that lowering the β_2 subunit expression reduces the "window current" area with potential therapeutic effects.

We designed a short hairpin RNA (shRNA) against $Ca_v\beta_2$ that targets both the endogenous $Ca_v\beta_{2a}$ and $Ca_v\beta_{2b}$ subunits. Recombinant adenoviruses, an effective system for delivering shRNA into the target cell (Benihoud *et al*., 1999; Hosono *et al*., 2004, 2005; Motegi *et al*., 2011), were used to transfect human embryonic kidney (HEK) cells, where a sufficient titer of adenoviruses could be generated and harvested from. The harvested adenoviruses, both β_2 shRNA-GFP and GFP only (no shRNA) were used to infect freshly dissociated rabbit ventricular myocytes. After 24-48 hours of incubation, the myocytes were examined under a fluorescence

microscope and only myocytes expressing GFP, as illustrated in fig. 8E and F, were included in subsequent electrophysiological experiments. To ensure that the shRNA we designed selectively knocks down the β_{2a} subunits without greatly affecting other β isoforms, we quantify the mRNA levels of β_2 subunits in rabbit ventricular myocytes infected with β_2 shRNA-GFP after 24-48 hr of incubation period. The levels of β_{2a} and β_{2b} subunit mRNA transcripts in myocytes infected with β_2 shRNA-GFP were both lower compared to those infected with GFP only (Fig. 9). Both β_{2a} and β_{2b} were reduced because the shRNA we designed for knocking down β_{2a} also targets the same region of gene encoding for β_{2b}. An increase in the expression of β_3 mRNA transcript in myocytes infected with β_2 shRNA-GFP compared to myocytes infected with GFP only, as seen in figure 9, could be a compensatory mechanism that the myocytes expressed to allow for LTCCs to be expressed and trafficked to the cell membrane despite the silenced β_{2a} and β_{2b} subunits.

Down-regulation of $Ca_v\beta_2$ subunits in rabbit ventricular myocytes prevents EAD formation.

Based on the findings mentioned so far, along with the levels of $Ca_v\beta_{2a}$ and $Ca_v\beta_{2b}$ mRNA transcripts being effectively reduced by infection with $Ca_v\beta_2$ shRNA, we tested the hypothesis that the decreased β_2 expression level reduces the overall "window current" region that has been implicated in EAD genesis, thus suppressing EADs and related arrhythmias. Myocytes expressing GFP (Fig. 8E, F), after being examined under a fluorescence microscope, were selected for electrophysiological experiments. Fig. 10 shows representative traces of the cardiac APs recorded in regular Tyrode's buffer solution and after perfusion of Tyrode's solution containing 0.6 mM H_2O_2. APs recorded from myocytes infected with GFP only exhibited EADs in H_2O_2 as shown on fig. 10B; on the other hand, myocytes with silenced $Ca_v\beta_2$ subunits showed

no EADs in H_2O_2 (Fig. 10C). The percentage of APs showing EADs (% EADs) was 0% in myocytes infected with β_{2a} shRNA-GFP compared to myocytes infected with GFP only having 32.6±6.1% EADs as shown in fig. 11C.

Reducing the levels of $Ca_v\beta_2$ mRNA transcripts also showed similar AP durations measured at 90% repolarization (APD_{90}) in H_2O_2 in each cell, with a mean of 0.151±0.027s, as compared to the mean APD in Tyrode's solution, 0.144±0.024s (Fig. 11A). On the contrary, the control myocytes infected with GFP alone exhibited longer APD_{90} in every cell upon exposure to 0.6 mM H_2O_2, with a mean of 0.940±0.5s, as compared to the APDs recorded in regular Tyrode's solution, 0.157±0.02s (Fig. 11B). These results suggest that ventricular myocytes with lower expression of β_2 subunits are more resistant to EAD formation and able to resist prolongation of APD as well. The $I_{Ca,L}$ amplitudes were then measured at various membrane potentials and were plotted in fig 12A. The steady state of activation and inactivation curves of $I_{Ca,L}$ were also plotted in fig. 12B. Fig. 12A shows that the reduction in β_2 subunits did not significantly alter the maximum $I_{Ca,L}$ density when compared between myocytes with (6.61±0.81pA/pF) and without $Ca_v\beta_2$ knockdown (6.67±0.51 pA/pF). This suggests that the reduction in β_2 mRNA transcripts did not affect the overall expression and functions of LTCCs on the plasma membrane. Despite the unchanged current density, we observed a shift in the half-activation and half-inactivation potentials of the steady state curves, ~3 mV to the right and ~2 mV to the left, respectively (Fig. 12B). Our results showed an overall reduction of the "window current" region by the shifts in the half-activation and half-inactivation curves in myocytes with down-regulated β_2. We propose that these shifts were potent enough to provide resistance to EADs in myocytes with silenced β_2 subunits. These results recapitulated the findings of Madhvani and colleagues that minimal

changes in the half-activation of the steady state activation and inactivation curves can potently suppress EADs (Madhvani *et al*., 2011).

Discussion

In this study, we 1) tested the relevance of LTCC biophysical properties in EAD genesis and 2) identified strategies to suppress the occurrence of EADs. Understanding the mechanisms involved in EAD formation is critical in providing insights for therapeutic strategies to prevent EAD-induced cardiac arrhythmias such as VF. In all experiments, we used H_2O_2, an oxidative stressor, to induce EADs in rabbit ventricular myocytes. To test the relevance of the non-inactivating component of $I_{Ca,L}$ in determining the size of the "window current" region implicated in EAD genesis, we used dynamic clamp technique to selectively alter that variable in ventricular myocytes exhibiting H_2O_2-induced EADs. We injected a virtual $I_{Ca,L}$ with modifiable biophysical properties after removing endogenous $I_{Ca,L}$ by blocking LTCC with nifedipine. Our results showed that lowering the non-inactivating component of $I_{Ca,L}$ profoundly suppressed EADs and restored APD to the physiological range (Fig. 6). These results suggest that the non-inactivating component of $I_{Ca,L}$ plays a major role in EAD genesis and could give insights to therapeutic strategies targeting specifically this biophysical property of LTCC.

Based on previous findings that β subunits modulate the biophysical properties of LTCC (Perez-Reyes *et al*., 1992; Birnbaumer *et al*., 1998; Dolphin, 2003, 2012), and on the findings of Olcese and colleagues that different β subunits modify the inactivating component of Ca^{2+} channels, we sought to explore the possible correlation between β subunits modulation and the non-inactivating component of $I_{Ca,L}$. As shown in fig. 7, β_{2a} subunits contribute to a higher non-inactivating component of $I_{Ca,L}$ than β_3 subunits do. We tested the hypothesis that lowering the levels of endogenous β_2 subunits increases the resistance of myocytes to the effects of H_2O_2 in generation of EADs. Our findings show that knocking down β_2 subunits could be a potent strategy to prevent EAD formation (Fig. 10 and 11) without causing any changes in the current

density of $I_{Ca,L}$ (Fig. 12A). This seems to prove to be a more favorable approach to preventing EADs because functional LTCCs are necessary for providing the major passageway for Ca^{2+} entry into the cell and Ca^{2+} signaling in the cell is critical for muscle contraction.

Furthermore, our results show that lowering the levels of β_2 subunits affected the biophysical properties of LTCC such that the half-activation and half-inactivation potentials of the steady state curves were shifted to the right and to the left, respectively. This finding supports the conclusions derived from the study by Madhvani and colleagues that EADs are sensitive to the change in half-activation and half-inactivation potentials. The authors have shown that a 4-5 mV shift in both potentials, such that the size of the "window current" regions is reduced, were potent to suppress EADs (Madhvani *et al*., 2011). While we were expecting to see also changes in the non-inactivating component of $I_{Ca,L}$, the results show no statistical difference (Fig. 12B). It is possible that the lack of statistical significance is due to the lower number of observations (n=3). Further experiments are necessary to validate this result.

In conclusion, according to our data, $Ca_v\beta_2$ subunits seem to be a potent target for a gene therapy-based antiarrhythmic strategy that could effectively suppress EAD-induced arrhythmias. While gene therapy is not yet applicable, I believe that this will likely be a important aspect of the medical field in the future years as technologies continue to advance in this field. Alternatively, the modification of LTCC properties that we have identified being therapeutically useful could be targeted pharmacologically. For example, using drugs that are able to alter the voltage-dependency of $I_{Ca,L}$ or to lower the $Ca_v\beta_2$ subunit levels in cardiomyocytes.

Our findings have demonstrated the potential profound use of gene therapy to target the modulatory subunits of LTCC, altering its composition to reduce EAD genesis in myocardium, without giving rise to any side effects that a pharmacological agent normally would.

Limitations

The most important limitation of this study is that, to achieve sufficient silencing of the β_2 subunits, the myocytes have to be maintained in culture for 24-48hr. While this is a necessary step to deliver or remove a gene of interest in a cell with a recombinant adenovirus, I recognize that some morphological and functional changes were observed (i.e. rounding of the edges of the ventricular myocytes and reduction in AP duration). Nevertheless, we have compared myocytes under identical culturing conditions for both control and β_2 knockdown myocytes and observed a clear resistance to EADs in β_2 knockdown myocytes compared to the control. Moreover, it will be of a primary importance to validate the results we observed in cultured myocytes in an intact heart. A possible area of study to be explored is a conditional knockout of β_{2a} subunits in an animal model, to see if the conclusion derived from our data in this thesis would apply to the animal.

Another limitation of this study is that in our dynamic clamp experiments, the Ca^{2+} currents were computer-simulated, and that it does not trigger Ca^{2+}-induced Ca^{2+} release from the SR. The effects of a real intracellular Ca^{2+} transient on Ca^{2+} sensitive currents affecting repolarization of the myocyte cannot be accounted for. Despite this limitation, we believe that this approach is a useful approach to identify selective aspects of an ion channel function to bring the field closer to a therapeutic discovery.

Figures

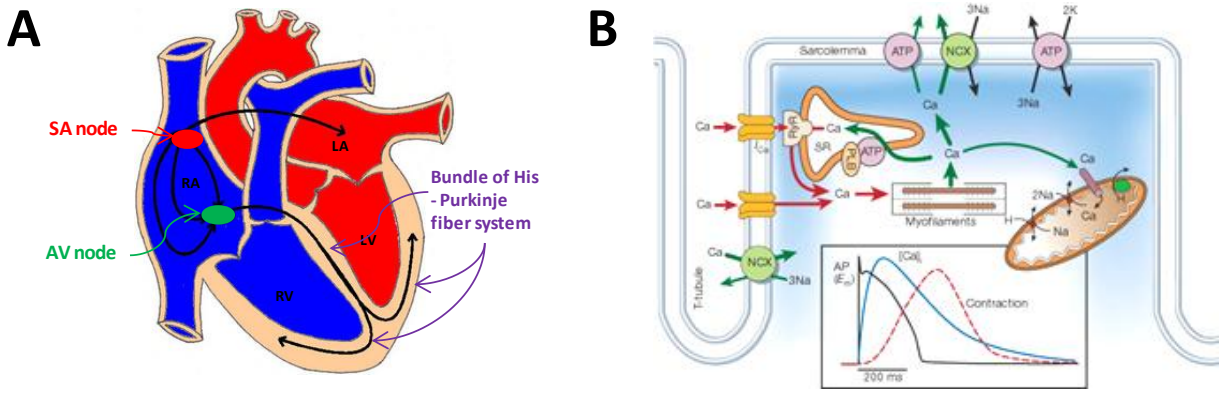

Bers DM. *Nature*. 2002; 415(6868):198-205

Figure 1. Electrical conduction of the heart and the dynamic interactions within a cardiomyocyte in response to Ca^{2+}.

A) A cartoon representation of a heart showing the electrical conduction initiated at sinoatrial (SA) node to atrioventricular (AV) node, which precede atrial contraction, and to the bundle of His-Purkinje fiber system. The ventricles contract when the electrical conduction propagates down the fiber system as the atria relax. B) The diagram represents the interactions between different proteins in Ca^{2+} signaling in a ventricular myocyte. NCX is Na+/Ca2+ exchanger, ATP is Na/K ATPase, PLB is phospholamban, SR, sarcoplasmic reticulum. The main entryway of Ca^{2+} from the extracellular medium is the L-type Ca^{2+} channels shown in orange. The graphs in the box show, in black, a ventricular myocyte's AP; in blue the intracellular [Ca^{2+}] during the course of the AP; in red, the contraction of the cardiac muscle.

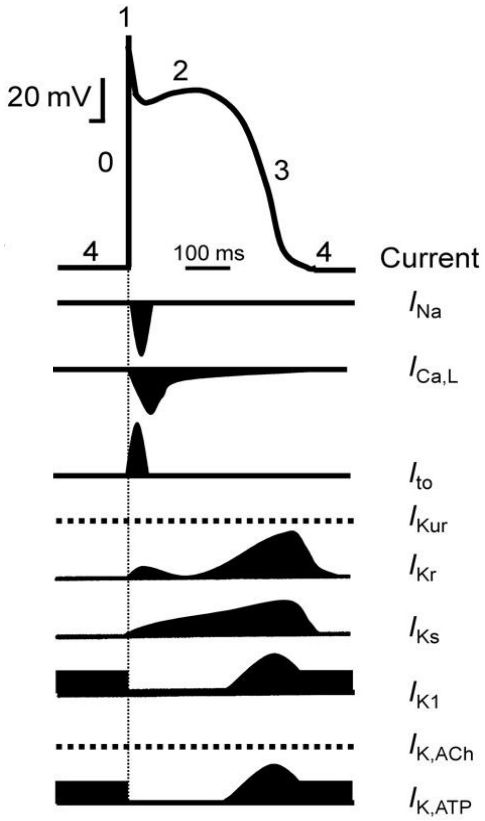

Adapted from Ravens U and Cerbai E. *Europace* 2008;10:1133-1137

Figure 2. Inward and outward currents that shape the ventricular action potential.

The top panel shows a ventricular action potential (AP) and the different phases that characterize the AP. Inward currents are mainly conducted by sodium and calcium channels; outward currents are mainly conducted by various potassium channels. Phase 0 shows a rapid depolarization; phase 1 shows a rapid early repolarization; phase 2 shows a slow 'plateau' of repolarization; phase 3 shows a rapid late repolarization; and phase 4 shows resting potential.

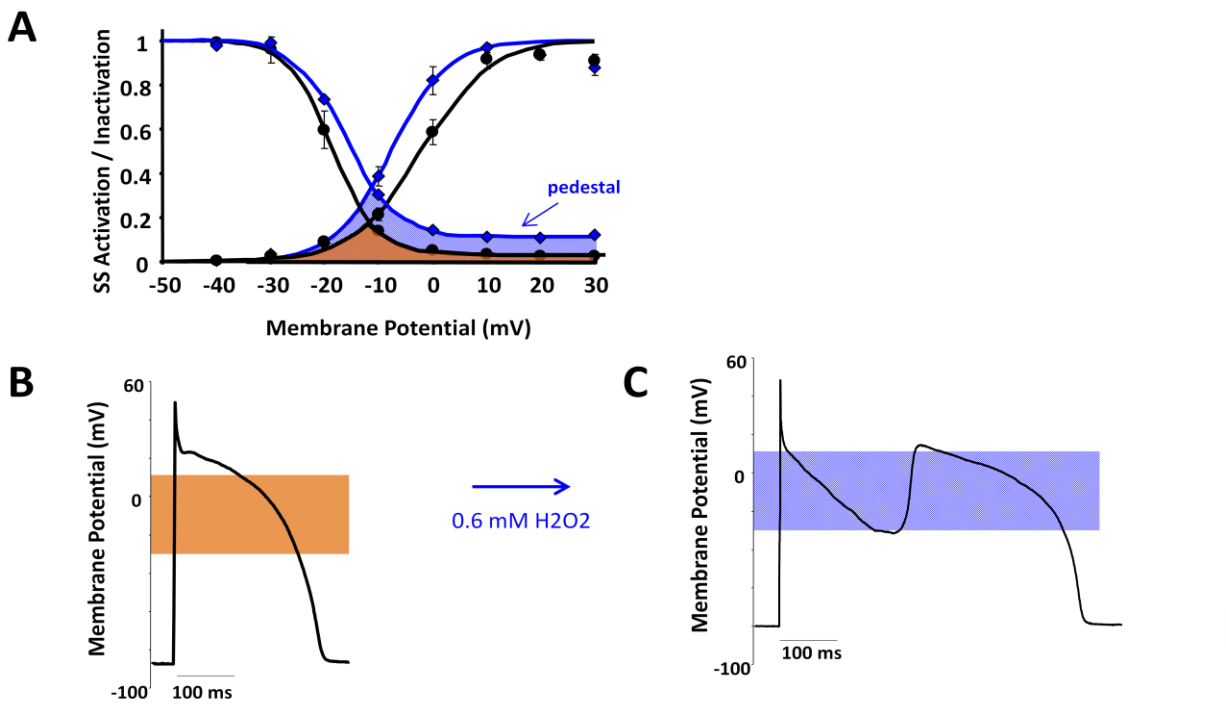

Figure 3. EAD formation occurs within the voltage range of "window current" region.

A) the black curves show the steady-state activation and inactivation curves of $I_{Ca,L}$ measured in rabbit ventricular myocytes in normal physiological Tyrode's buffer solution. The blue curves show the steady-state activation and inactivation curves of $I_{Ca,L}$ after being exposed to 0.6 mM H_2O_2. The shaded areas are known as the "window current" region, which is the region where steady state activation and inactivation curves overlap. B) A healthy rabbit ventricular cardiac action potential (AP), recorded at ~36-37°C in Tyrode's solution. C) A cardiac AP with EADS recorded in 0.6 mM H_2O_2. The orange shaded area and the blue dashed area in (B) and (C), respectively, reflect the "window current" regions of (A). This is showing that EAD often occurs within the "window current" region, between approximately -30 mV and +10 mV.

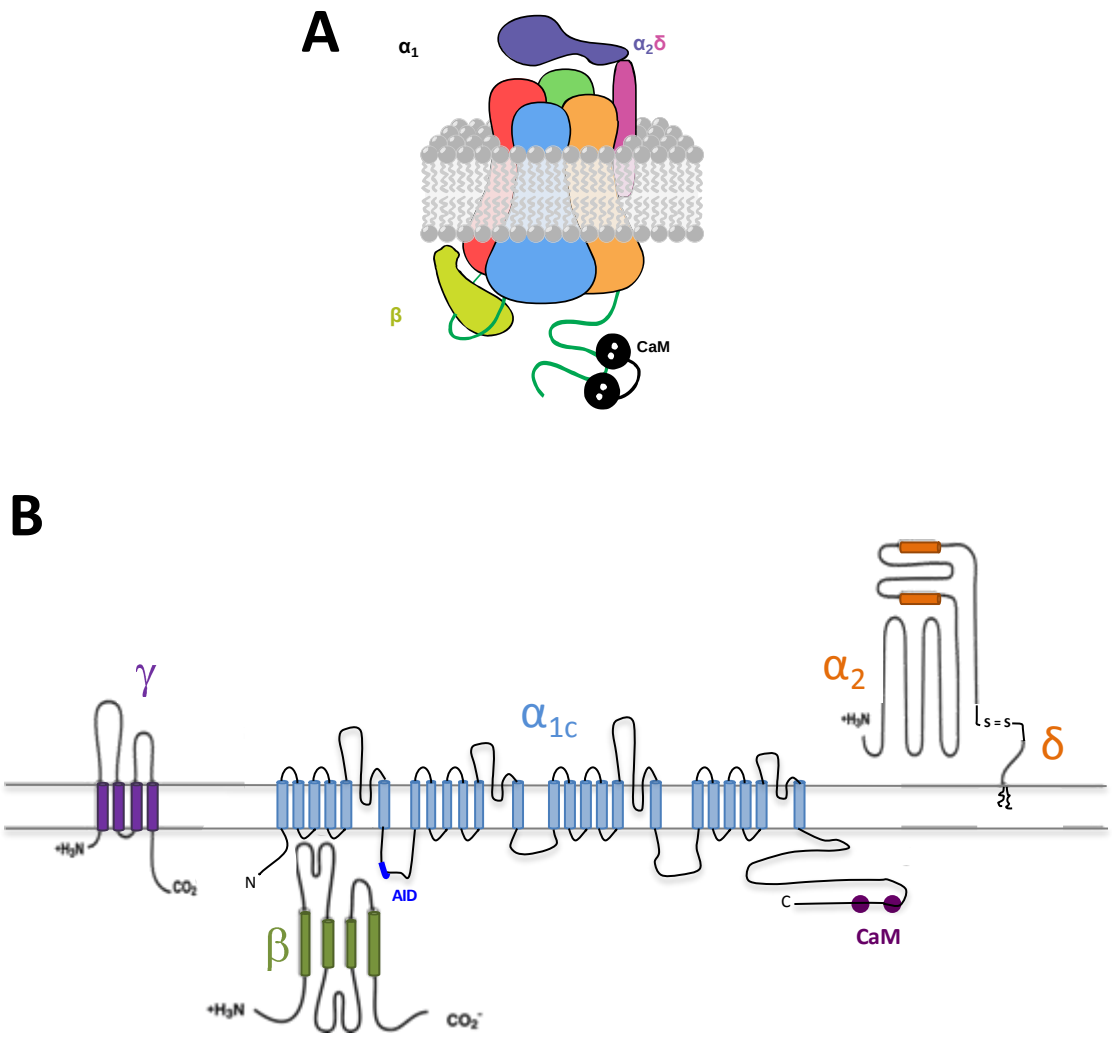

Adapted from William A. Catterall. *Cold Spring Harb Perspect Biol.* 2011; 3(8):a003947

Figure 4. Calcium channel topology.

A) 3-dimensional representation of an L-type calcium channel with the α1 being the pore-forming subunit with four distinct repeats (red, blue, orange, and green). The auxiliary subunits $\alpha_2\delta$ in purple and magenta and β in lime green are shown to interact with the α_1 subunit extracellularly and intracellularly, respectively. Calmodulin (CaM) is constitutively bound to the intracellular C-terminal region of the α_1 subunit. B) The topology of the LTCC reveals the different segments within each subunit. α_1 has 24 transmembrane segments, with α-interaction domain (AID) interacting with β subunit shown in green. CaM (in purple) is calmodulin where Ca^{2+} binds; it is located near the carboxy terminus. $\alpha_2\delta$ subunit is shown in orange; the δ part anchored to the plasma membrane via glycophosphatidylinositol, α_2 and δ are connected via a disulfide bridge (S=S). γ subunit shown in purple is composed of four transmembrane segments.

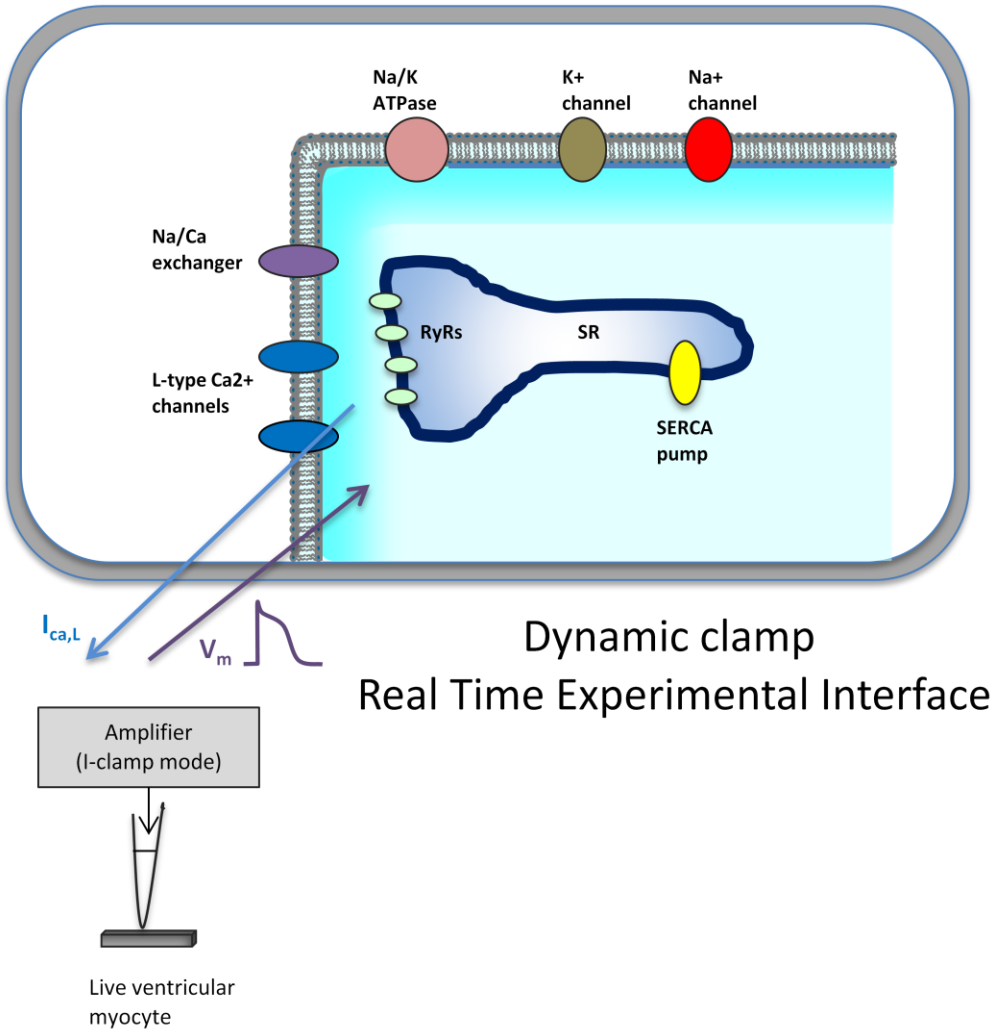

Figure 5. Dynamic Clamp system.

The diagram above illustrates a schematic of our dynamic clamp setup. Ventricular myocytes membrane potential recorded live is converted into a digital signal that is fed into the model (purple arrow) computed in real-time on real-time experimental interface (RTXI). On RTXI are the parameters, which shape the virtual $I_{Ca,L}$, that have been calculated and are modifiable. The $I_{Ca,L}$ (blue arrow) from the computer is converted from a digital to analogue signal and is injected into the cell (illustrated in the rectangular box), and is adjusted by the constant feedback of the cell's Vm in current-clamp mode in real-time. $I_{Ca,L}$ that is fed into the cell mimics the endogenous $I_{Ca,L}$ that has been removed by using nifedipine and to reconstitute the H_2O_2-induced EADs.

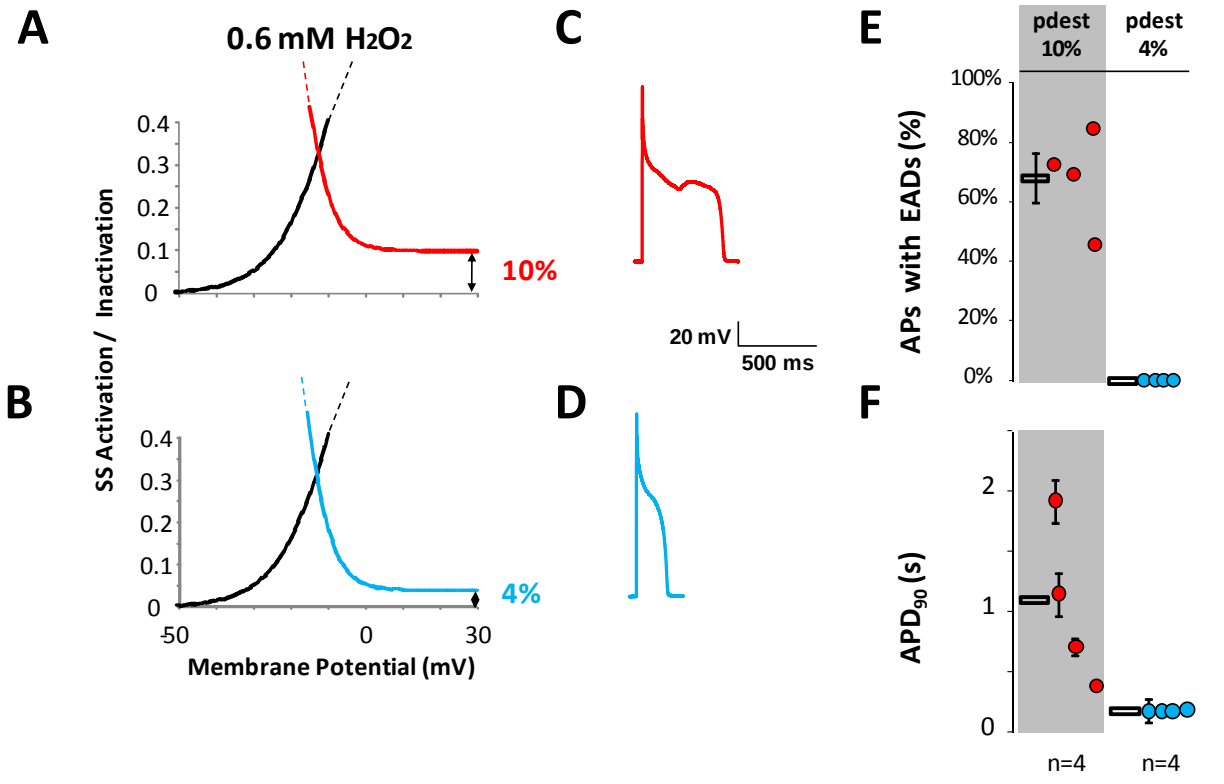

Figure 6. A reduction in the non-inactivating (pedestal) $I_{Ca,L}$ potently suppresses EADs and restores APD.

A, B) Enlarged view of the steady-state activation and inactivation curves of $I_{Ca,L}$ shows changes made to the non-inactivating component (pedestal). Under dynamic clamp and in the presence of 0.6 mM H_2O_2 and 20 µL nifedipine, we evaluated the effect of lowering the non-inactivating pedestal from 10% (A) to 4% of the peak current (B). C) Representative AP recorded in dynamic clamp under the condition show in (A). Note AP prolongation and EADs. Lowering the pedestal current to 4% (B) eliminates EADs and restores a normal APD (D). E) The percent of APs displaying EADs under two different pedestal amplitudes; pedestal of 10% in red, pedestal of 4% in blue. F) APD_{90} under two different pedestal amplitudes. Individual experiments are shown as solid circles; the means for all experiments are plotted as open rectangles. Error bars indicate SEM.

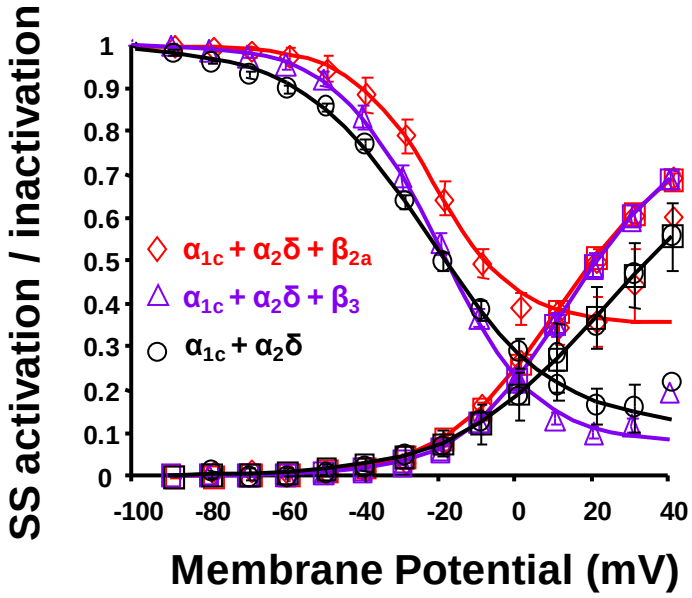

Figure 7. β subunits contribute to channel inactivation at different degrees. Steady state activation and inactivation curves above were calculated from the currents recorded in *Xenopus* oocytes expressing different subunit compositions of LTCC. The pore-forming α_{1c} was coexpressed with $\alpha_2\delta$ only (black circles), with $\alpha_2\delta$ and β_{2a} (red diamonds), and with $\alpha_2\delta$ and β_3 (purple triangles). The figure shows that β subunits shift the activation curve toward more negative potentials, and that the various isoforms of β subunits modulate the non-inactivating component of $I_{Ca,L}$ differently.

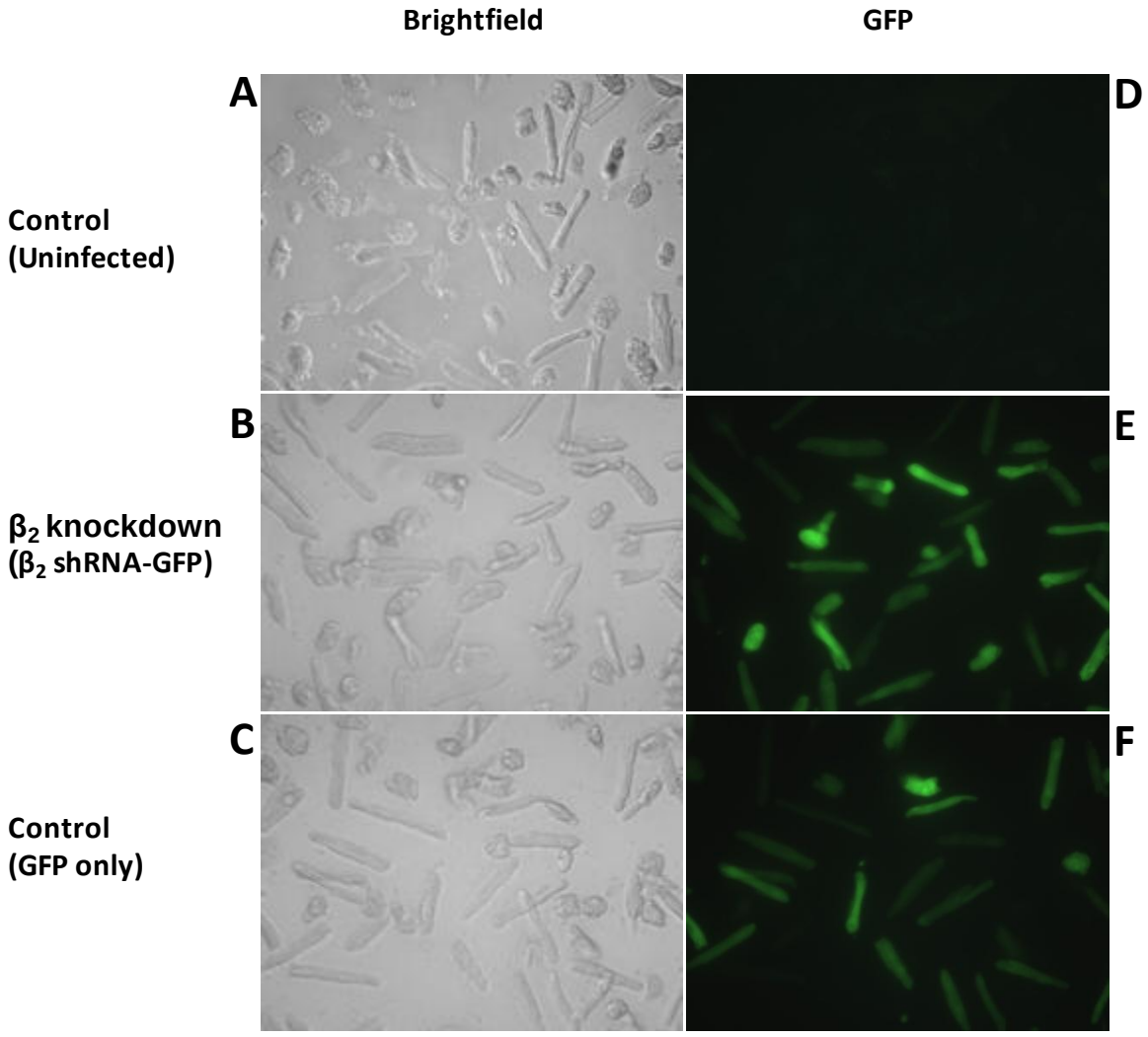

Figure 8. Myocytes infected with GFP-tagged viruses showed expression after 24-48 hr of incubation.

The rabbit ventricular myocytes were plated on a coating protein, geltrex, following isolation, and infected with 10 µL of virus per 1 mL of media. They were then incubated for 24-48 hr to allow for β_2 down-regulation. Only GFP-fluorescing myocytes were included for subsequent electrophysiological experiments. A) an image taken with brightfield microscopy of uninfected cultured myocytes showed no GFP fluorescence in (D). B) an image taken with brightfield microscopy of myocytes infected with β_2 shRNA-GFP showing green in (E) under fluorescence microscopy. C) an image taken with brightfield microscopy of myocytes infected with GFP only showing green as seen in (F) under fluorescence microscopy.

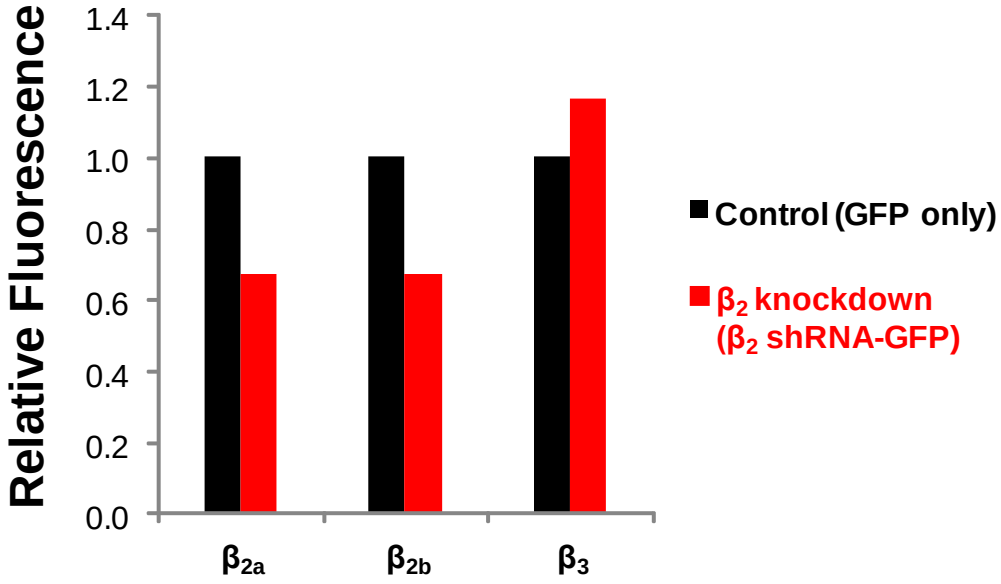

Figure 9. RT-PCR quantifies the reduction in β_2 concentrations in rabbit ventricular myocytes upon infection with adenovirus containing β_2 shRNA construct.

The bar graph above represents the quantitative analysis of the relative expressions of various β isoforms: β_{2a}, β_{2b}, and β_3, measured from the total mRNA extracted from rabbit ventricular myocytes infected with GFP only and myocytes infected with β_2 shRNA-GFP. The levels of relative fluorescence of $\beta_{2a,}$ β_{2b}, and β_3 subunits for each empty-GFP and β_2 shRNA-GFP were normalized against GADPH fluorescence. The total mRNA were extracted from rabbit ventricular myocytes and quantified after 24-48 hr of incubation at 37°C following viral infections of 10 µL of virus per 1 mL medium. The bars in black show relative fluorescence in myocytes infected with GFP alone, those in red show relative fluorescence in myocytes infected with β_2 shRNA-GFP. Note that β_2 shRNA lowered the relative expression of both β_{2a} and β_{2b} while increasing β_3 relative expression.

.

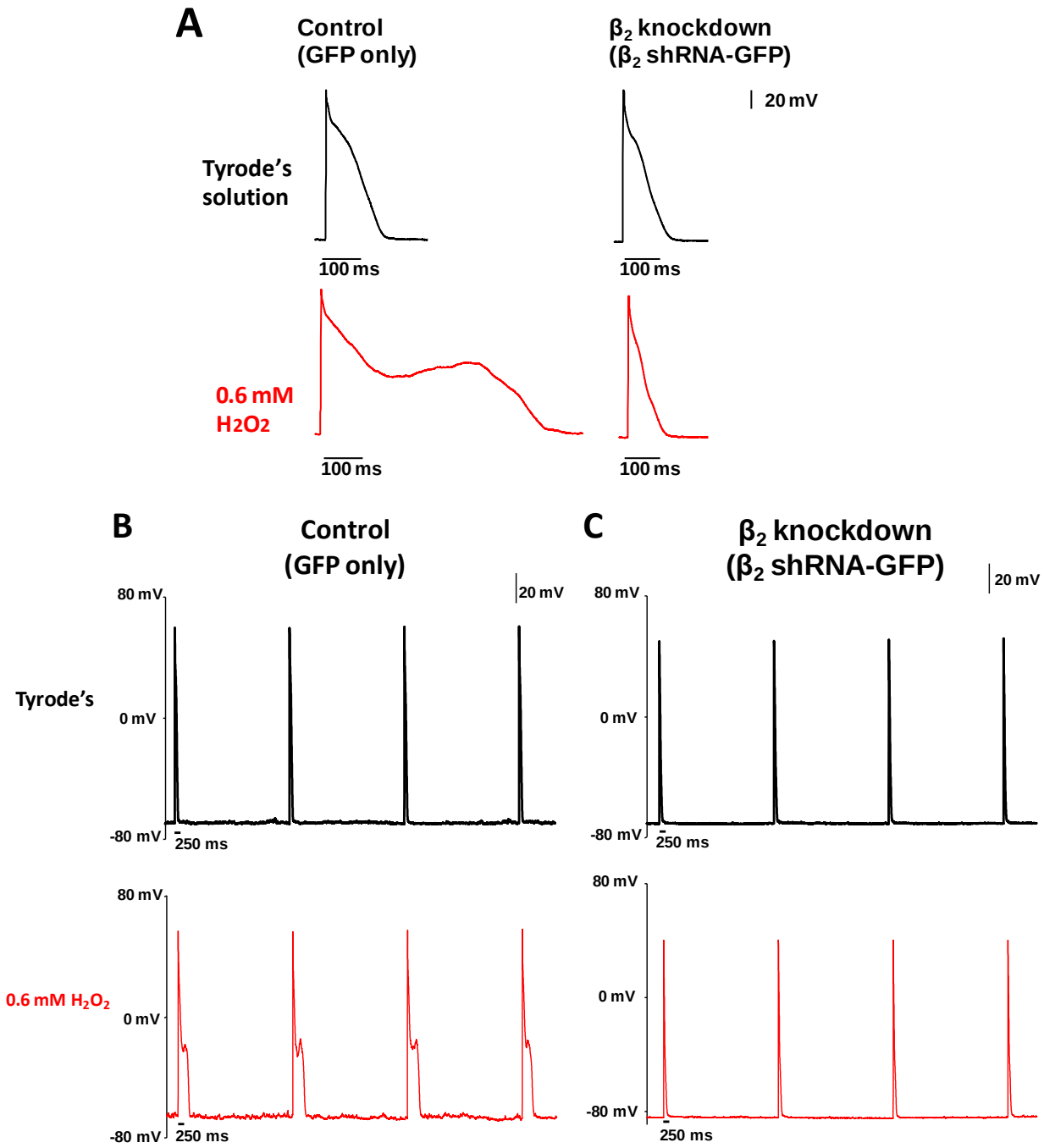

Figure 10. Silencing β_2 subunit modulates Ca^{2+} channel biophysical properties, making rabbit ventricular myocytes more resistant to EADs.

A) representative single traces of cardiac action potentials (APs) all recorded in Tyrode's buffer solution (top, black) with subsequent superfusion of 0.6 mM H_2O_2 (bottom, red). All recordings were done at 34-36°C, paced at 5 s cycle lengths. B,C) trains of four consecutive APs recorded from rabbit ventricular myocytes after infections with either GFP only (B) or β_2 shRNA-GFP. The myocytes were cultured for 24-48 hr at 37°C. Black traces show the APs when the cells were bathed in Tyrode's buffer solution, the red traces show the APs in the presence of 0.6 mM H_2O_2. Note that the myocytes infected with β_2 shRNA-GFP showed no EADs; whereas, the myocytes infected with GFP only showed EADs in 0.6 mM H_2O_2.

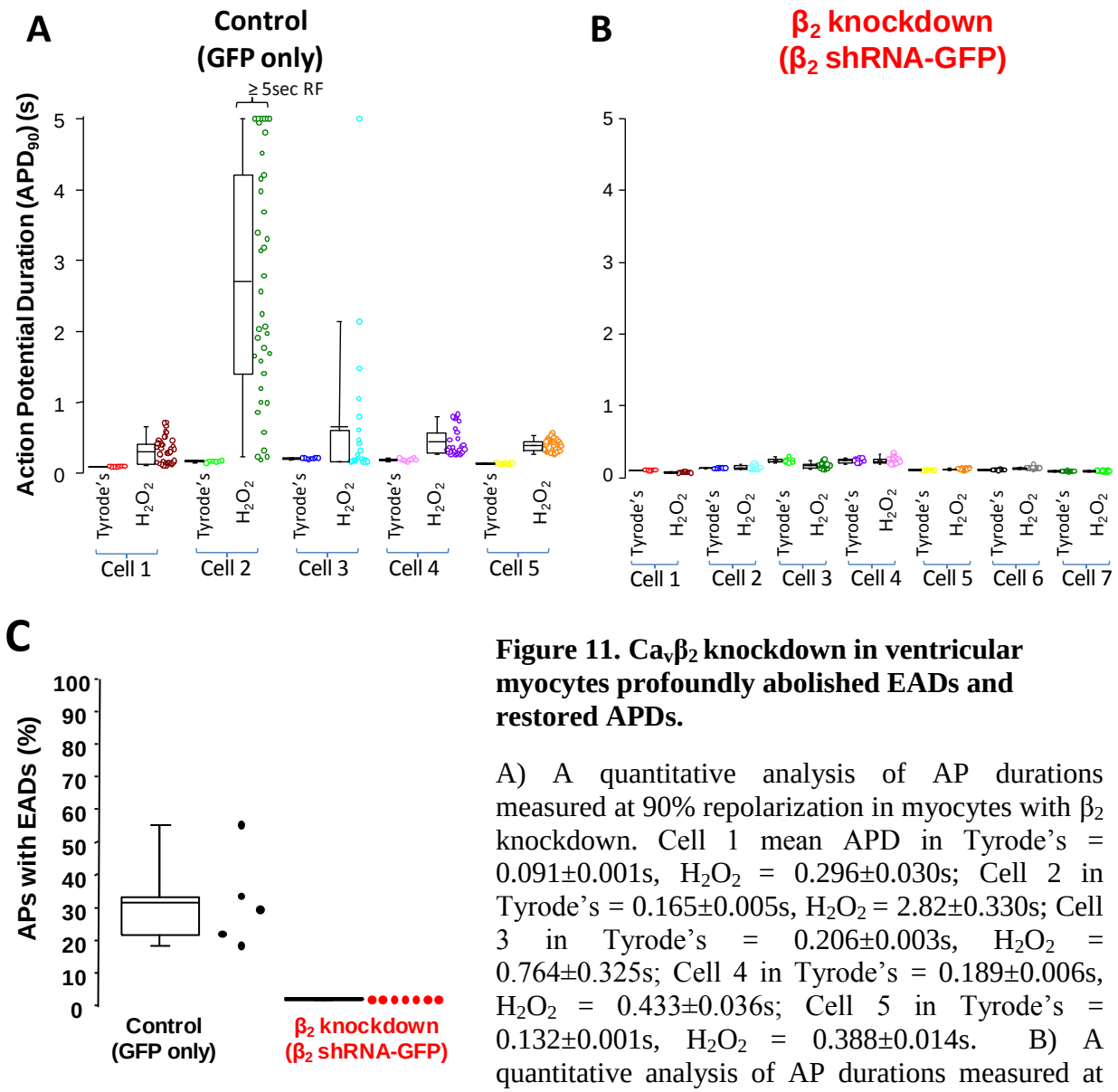

Figure 11. $Ca_v\beta_2$ knockdown in ventricular myocytes profoundly abolished EADs and restored APDs.

A) A quantitative analysis of AP durations measured at 90% repolarization in myocytes with β_2 knockdown. Cell 1 mean APD in Tyrode's = 0.091±0.001s, H_2O_2 = 0.296±0.030s; Cell 2 in Tyrode's = 0.165±0.005s, H_2O_2 = 2.82±0.330s; Cell 3 in Tyrode's = 0.206±0.003s, H_2O_2 = 0.764±0.325s; Cell 4 in Tyrode's = 0.189±0.006s, H_2O_2 = 0.433±0.036s; Cell 5 in Tyrode's = 0.132±0.001s, H_2O_2 = 0.388±0.014s. B) A quantitative analysis of AP durations measured at 90% repolarization in control myocytes infected with GFP only. Cell 1 mean APD in Tyrode's = 0.105±0.001s, H_2O_2 = 0.073±0.001s; Cell 2 in Tyrode's = 0.132±0.002s, H_2O_2 = 0.142±0.005s; Cell 3 in Tyrode's = 0.234±0.011s, H_2O_2 = 0.262±0.045s; Cell 4 in Tyrode's = 0.235±0.008s, H_2O_2 = 0.234±0.008s; Cell 5 in Tyrode's = 0.105±0.001s, H_2O_2 = 0.121±0.002s; Cell 6 in Tyrode's = 0.107±0.001, H_2O_2 = 0.131±0.001s; Cell 7 in Tyrode's = 0.090±0.001, H_2O_2 = 0.091±0.001s. A,B) Each dot represent the APD of a single action potential. The boxes represent the range of % APs with EADs, the horizontal lines represent the mean, and the whiskers, the interquantile range, indicate the 5th and 95th percentiles. The experiments were done in 0.6 mM H_2O_2 at 34-36°C. For each control cell there is a β_{2a}-GFP infected cell from the same batch, all cells being cultured in the same condition and infected with the same virus concentrations. C) Quantitative analysis of % APs with EADs recorded from rabbit ventricular myocytes each dot represents individual experiments. Black dots: GFP only, n=5; red dots: β_{2a}-GFP shRNA, n=7. The mean %EADs in the control is 32.6±6.1%. Note that the control cells show higher % EADs in (C) and longer APDs when exposed to H_2O_2 (A) as compared to the β_2 knockdown cells (B).

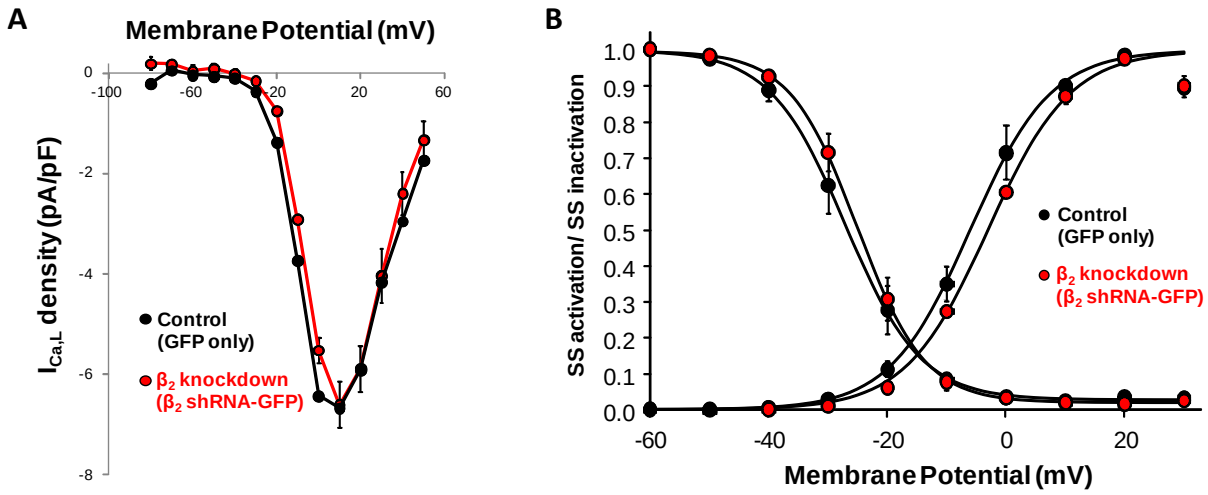

Figure 12. Reduction in $Ca_v\beta_2$ subunits did not alter the peak current density of $I_{Ca,L}$ but modified its steady state properties in rabbit ventricular myocytes

A)) I-V curve of $I_{Ca,L}$ normalized to the peak current. The black dots represent myocytes infected with GFP only; the red dots represent myocytes infected with β_{2a}-GFP shRNA viruses (n=3). Control myocytes had $I_{Ca,L}$ density of 6.67±0.51 pA/pF, β_{2a} knockdown myocytes had $I_{Ca,L}$ density of 6.61±0.81pA/pF. B) steady state activation/inactivation curves of ICa,L. The black dotted curves represent the steady state curves of myocytes infected with empty-GFP viruses as controls. The red dotted curves represent the steady state curves of myocytes infected with β_{2a}-GFP shRNA viruses. Recordings were obtained at 34–36°C. The reduction in β_2 subunits did not significantly reduce the overall $I_{Ca,L}$ density in ventricular myocytes; but it shifted the steady state activation curve to the right by ~4 mV and the steady state inactivation to the left by ~2 mV.

Bibliography

Arikkath J, Campbell KP. Auxiliary subunits: essential components of the voltage-gated calcium channel complex. *Current Opinion in Neurobiology.* 2003; 13 (3); 298–307.

Benihoud K, Yeh P, Perricaudet M. Adenovirus vectors for gene delivery. *Curr Opin Biotechnol*. 1999; 10(5):440-7.

Berecki G, Zegers JG, Verkerk AO, Bhuiyan ZA, de Jonge B, Veldkamp MW, Wilders R, Van Ginneken AC. HERG channel (dys)function revealed by dynamic action potential clamp technique. *Biophys J.* 2005;88:566–578.

Berecki G, Zegers JG, Bhuiyan ZA, Verkerk AO, Wilders R, Van Ginneken AC. Long-QT syndrome-related sodium channel mutations probed by the dynamic action potential clamp technique. *J Physiol.* 2006;570:237–250.

Berecki G, Zegers JG, Wilders R, Van Ginneken AC. Cardiac channelopathies studied with the dynamic action potential-clamp technique. *Methods Mol Biol.* 2007;403:233–250.

Bers DM. Excitation-contraction coupling and cardiac contractile force. 2nd Ed. *Kluwer Academic Publishers*, 2001.

Bers DM. Cardiac excitation-contraction coupling. *Nature.* 2002; 415(6868):198-205.

Bers DM, Guo T. Calcium signaling in cardiac ventricular myocytes. *Ann N Y Acad Sci*. 2005; 1047:86-98.

Birnbaumer L, Qin N, Olcese R, Tareilus E, Platano D, Costantin J, Stefani E. Structures and functions of calcium channel beta subunits. *J Bioenerg Biomembr*. 1998;30:357–375.

Buraei Z, Jian Yang. Structure and function of the β subunit of voltage-gated Ca2+ channels. *Biochim Biophys Acta.* 2013; 1828(7): 1530–1540.

Catterall WA, Few AP. Calcium channel regulation and presynaptic plasticity. *Neuron.* 2008; 59: 882–901.

Catterall WA. Voltage-gated calcium channels. *Cold Spring Harb Perspect Biol.* 2011; 3(8):a003947.

Clusin WT. Calcium and Cardiac Arrhythmias: DADs, EADs, and Alternans. *Critical Reviews in Clinical Laboratory Sciences*. 2003; 40(3):337–375.

Colecraft HM, Alseikhan B, Takahashi SX, Chaudhuri D, Mittman S, Yegnasubramanian V, Alvania RS, Johns DC, Marban E, Yue DT. Novel functional properties of Ca(2+) channel beta subunits revealed by their expression in adult rat heart cells. *J Physiol* 2002; 541(Pt 2):435-52.

Cranefield PF, Wit AL, Hoffman BF. Conduction of the Cardiac Impulse. *J Gen Physiol*. 1972; 59(2): 227–246.

Cranefield PF, Aronson RS. Initiation of sustained rhythmic activity by single propagated action potentials in canine cardiac Purkinje fibers exposed to sodium-free solution or to ouabain. *Circ Res*. 1974; 34(4):477-81.

Cranefield PF. Action potentials, afterpotentials, and arrhythmias. *Circ Res*. 1977; 41(4):415-23.

Davies A, Kadurin I, Alvarez-Laviada A, Douglas L, Nieto-Rostro M, Bauer CS, Pratt WS, Dolphin AC. The alpha2delta subunits of voltage-gated calcium channels form GPI-anchored proteins, a posttranslational modification essential for function. *Proc Natl Acad Sci U S A*. 2010; 107(4):1654-9.

Deng Y, Wang CC, Choy KW, Du Q, Chen J, Wang Q, Li L, Chung TK, Tang T. Therapeutic potentials of gene silencing by RNA interference: principles, challenges, and new strategies. *Gene*. 2014; 538(2):217-27.

Dolphin A. β Subunits of Voltage-Gated Calcium Channels. *J Bioenerg Biomemb*.2003; 35(6): 599-620.

Dolphin A. Calcium channel auxiliary $\alpha_2\delta$ and β subunits: trafficking and one step beyond. *Nature Reviews Neuroscience*. 2012; 13, 542-555.

Fire A, Xu S, Montgomery MK, Kostas SA, Driver SE, Mello CC. Potent and specific genetic interference by double-stranded RNA in Caenorhabditis elegans. *Nature.* 1998; 391(6669):806-11.

Flavell SW, Greenberg ME. Signaling mechanisms linking neuronal activity to gene expression and plasticity of the nervous system. *Annu Rev Neurosci.* 2008; 31: 563–590.

Gudzenko V, Shiferaw Y, Savalli N, Vyas R, Weiss JN, Olcese R. Influence of channel subunit composition on L-type Ca2+ current kinetics and cardiac wave stability. *Am J Physiol Heart Circ Physiol*. 2007; 293(3):H1805-H1815.

Gupta PK, Sonwane AA, Singh NK, Meshram CD, Dahiya SS, Pawar SS, Gupta SP, Chaturvedi VK, Saini M. Intracerebral delivery of small interfering RNAs (siRNAs) using adenoviral vector protects mice against lethal peripheral rabies challenge. *Virus Res*. 2012; 163(1):11-8.

Hirano Y, Moscucci A, January CT. Direct measurement of L-type Ca2+ window current in heart cells. *Circ Res*. 1992; 70(3):445-55.

Hosey MM, Chien AJ, Puri TS. Structure and regulation of L-type calcium channels a current assessment of the properties and roles of channel subunits. *Trends Cardiovasc Med*. 1996; 6(8):265-73.

Hosono T, Mizuguchi H, Katayama K, Xu ZL, Sakurai F, Ishii-Watabe A, Kawabata K, Yamaguchi T, Nakagawa S, Mayumi T, Hayakawa T. Adenovirus vector-mediated doxycycline-inducible RNA interference. *Hum Gene Ther*. 2004; 15(8):813-9.

Hosono T, Mizuguchi H, Katayama K, Koizumi N, Kawabata K, Yamaguchi T, Nakagawa S, Watanabe Y, Mayumi T, Hayakawa T. RNA interference of PPARgamma using fiber-modified adenovirus vector efficiently suppresses preadipocyte-to-adipocyte differentiation in 3T3-L1 cells. *Gene*. 2005; 348:157-65.

Hullin R, Matthes J, von Vietinghoff S, Bodi I, Rubio M, D'Souza K, Friedrich Khan I, Rottländer D, Hoppe UC, Mohacsi P, Schmitteckert E, Gilsbach R, Bünemann M, Hein L, Schwartz A, Herzig S. Increased expression of the auxiliary beta(2)-subunit of ventricular L-type Ca(2)+ channels leads to single-channel activity characteristic of heart failure. *PLoS One*. 2007; 2(3):e292.

January CT, Riddle JM. Early afterdepolarizations: mechanism of induction and block. A role for L-type Ca^{2+} current. *Circ Res*. 1989; 64:977–990.

January CT, Riddle JM, Salata JJ. A model for early afterdepolarizations: induction with the Ca^{2+} channel agonist Bay K 8644. *Circ Res.* 1988; 62(3):563-571.

John RM, Tedrow UB, Koplan BA, Albert CM, Epstein LM, Sweeney MO, Miller AL, Michaud GF, Stevenson WG. Ventricular arrhythmias and sudden cardiac death. *Lancet.* 2012; 380(9852):1520-9

Karagueuzian HS, Nguyen TP, Qu Z, Weiss JN. Oxidative stress, fibrosis, and early afterdepolarization-mediated cardiac arrhythmias. *Front. Physiol.* 2013; 4: 19.

Kirshenbaum LA, MacLellan WR, Mazur W, French BA, Schneider MD. Highly efficient gene transfer into adult ventricular myocytes by recombinant adenovirus. *J Clin Invest.* 1993; 92(1):381-7

Koval OM, Guan X, Wu J, Joiner ML, Gao Z, Chen B, Grumbach IM, Luczak ED, Colbran RJ, Song LS, Hund TJ, Mohler PT, Anderson ME. CaV1.2 beta-subunit coordinates CaMKII-triggered cardiomyocyte death and afterdepolarizations. *Proc Natl Acad Sci U S A.* 2010; 107(11): 4996–5000

Li B, Yang Y, Jiang S, Ni B, Chen K, Jiang L. Adenovirus-mediated overexpression of BMP-9 inhibits human osteosarcoma cell growth and migration through downregulation of the PI3K/AKT pathway. *Int J Oncol.* 2012; 41(5):1809-19.

Luo J, Deng Z, Luo X, Tang N, Song W, Chen J, Sharff KA, Luu HH, Haydon RC, Kinzler KW, Vogelstein B & He T. (2007). A protocol for rapid generation of recombinant adenoviruses using the AdEasy system. *Nature Protocols*. 2007; 2, 1236-1247

Madhvani RV, Xie Y, Pantazis A, Garfinkel A, Qu Z, Weiss JN. Shaping a new Ca2+ conductance to suppress early afterdepolarizations in cardiac myocytes. *J Physiol.* 2011; 589(Pt 24): 6081-6092.

Mahajan A, Sato D, Shiferaw Y, Baher A, Xie LH, Peralta R, Olcese R, Garfinkel A, Qu Z, Weiss JN. Modifying L-type calcium current kinetics: consequences for cardiac excitation and arrhythmia dynamics. *Biophys J*. 2008a; 94(2):411-23

Mahajan A, Shiferaw Y, Sato D, Baher A, Olcese R, Xie LH, Yang MJ, Chen PS, Restrepo JG, Karma A, Garfinkel A, Qu Z & Weiss JN. A rabbit ventricular action potential model replicating cardiac dynamics at rapid heart rates. *Biophys J*. 2008b; 94, 392–410.

Maltsev VA, Vinogradova TM, Lakatta EG. The emergence of a general theory of the initiation and strength of the heartbeat. *J Pharmacol Sci.* 2006; 100(5):338-69

Mizuno T, Chou MY, Inouye M. A unique mechanism regulating gene expression: Translational inhibition by a complementary RNA transcript (micRNA). *Proc Natl Acad Sci U S A*. 1984; 81:1966–70.

Motegi Y, Katayama K, Sakurai F, Kato T, Yamaguchi T, Matsui H, Takahashi M, Kawabata K, Mizuguchi H. An effective gene-knockdown using multiple shRNA-expressing adenovirus vectors. *J Control Release*. 2011; 153(2):149-53.

Neely A, Wei X, Olcese R, Birnbaumer L, Stefani E. Potentiation by the beta subunit of the ratio of the ionic current to the charge movement in the cardiac calcium channel. *Science.* 1993; 262(5133):575-8.

Olcese R, Qin N, Schneider T, Neely A, Wei X, Stefani E, Birnbaumer L. The amino terminus of a calcium channel beta subunit sets rates of channel inactivation independently of the subunit's effect on activation. *Neuron.* 1994; 13(6):1433-8

Ono K, Iijima T. Cardiac T-type Ca(2+) channels in the heart. *J Mol Cell Cardiol.* 2010; 48(1):65-70.

Ottolia M, Torres N, Bridge JH, Philipson KD, Goldhaber JI. Na/Ca exchange and contraction of the heart. *J Mol Cell Cardiol.* 2013; 61:28-33

Perez-Reyes E, Castellano A, Kim HS, Bertrand P, Baggstrom E, Lacerda AE, Wei XY, Birnbaumer L. Cloning and expression of a cardiac/brain beta subunit of the L-type calcium channel. *J Biol Chem.* 1992; 267(3):1792-7

Peterson BZ, DeMaria CD, Adelman JP, Yue DT. Calmodulin is the Ca2+ sensor for Ca2+ -dependent inactivation of L-type calcium channels. *Neuron.* 1999; 22(3):549-58.

Ravens U, Cerbai E. Role of potassium currents in cardiac arrhythmias. *Europace*. 2008;10:1133-1137

Sato D, Xie LH, Qu Z. Synchronization of chaotic early afterdepolarizations in the genesis of cardiac arrhythmias. *Proc. Natl. Acad. Sci. USA*. 2009;106:2983–2988

Shibata EF, Giles RW. Ionic currents that generate the spontaneous diastolic depolarization in individual cardiac pacemaker cells. *Proc. Natl. Acad. Sci. USA.* 1985; 82, 7796-7800

Singer D, Biel M, Lotan I, Flockerzi V, Hofmann F, Dascal N. The roles of the subunits in the function of the calcium channel. *Science* 1991; 253(5027):1553-7

Suckau L, Fechner H, Chemaly E, Krohn S, Hadri L, Kockskämper J, Westermann D, Bisping E, Ly H, Wang X, Kawase Y, Chen J, Liang L, Sipo I, Vetter R, Weger S, Kurreck J, Erdmann V, Tschope C, Pieske B, Lebeche D, Schultheiss HP, Hajjar RJ, Poller WC. Long-term cardiac-targeted RNA interference for the treatment of heart failure restores cardiac function and reduces pathological hypertrophy. *Circulation*. 2009; 119(9):1241-52

Tan RC, Joyner RW. Electrotonic influences on action potentials from isolated ventricular cells. *Circ. Res.* 1990; 67:1071-1081

Tanabe T, Takeshima H, Mikami A, Flockerzi V, Takahashi H, Kangawa K, Kojima M, Matsuo H, Hirose T, Numa S. Primary structure of the receptor for calcium channel blockers from skeletal muscle. *Nature.* 1987; 328(6128):313-8

Tsien RW, Lipscombe D, Madison DV, Bley KR, Fox AP. Multiple types of neuronal calcium channels and their selective modulation. *Cell Press.* 1988; 11(10):431-438

Verkhratsky A, Parpura V. History of electrophysiology and the patch clamp. *Methods Mol Biol*. 2014; 1183:1-19

Weiss JN, Garfinkel A, Karagueuzian H, Chen PS, Qu Z. Early afterdepolarizations and cardiac arrhythmias. *Heart Rhythm*. 2010; 7(12):1891-1899.

Wilders R. Dynamic clamp: a powerful tool in cardiac electrophysiology. *J Physiol.* 2006; 576:349–359.

Yang SN, Berggren PO. The role of voltage-gated calcium channels in pancreatic beta-cell physiology and pathophysiology. *Endocr Rev*. 2006;27(6):621-76